AGU ADVANCING EARTH AND SPACE SCIENCE

Water Resources Research

RESEARCH ARTICLE
10.1029/2020WR028582

Probabilistic Projections of Multidimensional Flood Risks at a Convection-Permitting Scale

B. Zhang[1], S. Wang[1,2], and Y. Wang[3]

[1]Department of Land Surveying and Geo-Informatics, The Hong Kong Polytechnic University, Hong Kong, China [2]Shenzhen Research Institute, The Hong Kong Polytechnic University, Shenzhen, China [3]Department of Atmospheric and Geological Sciences, State University of New York at Oswego, Oswego, NY, USA

Key Points:

- Probabilistic projections of multidimensional flood risks were developed at a convection-permitting scale
- High-resolution climate projections with the 4-km horizontal grid spacing were developed using the convection-permitting Weather Research and Forecasting model
- Bayesian vine copula approach was proposed to uncover potential interactions among flood variables and associated uncertainties

Supporting Information:

- Figure S1

Correspondence to:

S. Wang,
shuo.s.wang@polyu.edu.hk

Citation:

Zhang, B., Wang, S., & Wang, Y. (2021). Probabilistic projections of multidimensional flood risks at a convection-permitting scale. *Water Resources Research*, *57*, e2020WR028582. https://doi.org/10.1029/2020WR028582

Received 9 AUG 2020
Accepted 9 DEC 2020

Abstract Understanding future river flood risk is a prerequisite for developing climate change adaptation strategies and enhancing disaster resilience. Previous flood risk assessments can barely take into account future changes of fine-scale hydroclimatic characteristics and hardly quantify multivariate interactions among flood variables, thereby resulting in an unreliable assessment of flood risk. In this study, for the first time, we develop probabilistic projections of multidimensional river flood risks at a convection-permitting scale through the Weather Research and Forecasting (WRF) climate simulations with 4-km horizontal grid spacing. Vine copula has been widely used to assess the multidimensional dependence structure of hydroclimate variables, but the commonly used frequentist approach may fail to identify the correct vine model and to obtain the uncertainty interval. Thus, a Bayesian vine copula approach is proposed to explicitly address the multidimensional dependence of flood characteristics (i.e., flood peak, volume, and duration) and underlying uncertainties. The proposed approach enables a robust assessment of return periods of future floods for Guadalupe and Mission river basins located in South Texas of the United States. Our findings reveal that the South Texas region is projected to experience more flood events with longer duration and greater discharge volume. The flood peak, however, will not necessarily increase even though precipitation extremes are expected to become more frequent. The projected flood return periods over the Guadalupe river basin do not show an obvious increase while the Mission river basin is projected to face a dramatic increase in flood risk with exposed to 100-year and even severer floods nearly every 2 years, on average, when considering the combined effects of flood peak, volume, and duration.

1. Introduction

Floods are one of the major natural disasters inflicting catastrophic damages on society and ecosystems and even causing millions of deaths (Bevacqua et al., 2017; Carvalho & Wang, 2019; Mallakpour et al., 2019). The 2017 California floods, for example, forced evacuations for thousands of people, while the Mississippi River floods of 2019 caused up to $20 billion in economic losses and at least 12 deaths (Smith, 2020). The huge losses caused by floods confront all mankind with an urgent question: How severe future floods will be under climate change? To date no agreement has been reached on this issue (Blöschl et al., 2019; Marsooli et al., 2019; Sharma et al., 2018). A reliable projection of future changes in flood risks is therefore crucial for designing suitable flood protection structures and for enhancing resilience to climate-induced disasters.

The hydrologic predictions forced by the simulated climate variables (e.g., precipitation and temperature) have been widely used to assess flood risks under climate change. Previous climate simulations were conducted using general circulation models (GCMs) and regional climate models (RCMs) for assessing flood hazards (Alfieri et al., 2015; Hirabayashi et al., 2013; Jongman et al., 2015; Raff et al., 2009; Shkolnik et al., 2018; Winsemius et al., 2016). However, GCMs are too coarse (~100–300 km) to capture regional or local hydroclimatic characteristics. Although RCMs are largely improved in terms of the horizontal grid spacing (e.g., 10–50 km), they are not fine enough to explicitly resolve deep convection which is a critical subgrid process operating at scales from the microscale to the synoptic scale (Brisson et al., 2016; Fosser et al., 2014; Liu et al., 2017; Prein et al., 2013; Zhu et al., 2019). Thus, RCMs heavily rely on the convection parameterization schemes, leading to a misrepresentation of the diurnal cycle of convective precipitation and a large underestimation of hourly precipitation intensities (Chen et al., 2020a, 2020b; Giorgi, 2019; Wang & Wang, 2019; Zhang et al., 2019). Such underestimation can lead to a considerable bias in projecting future

flood risks. Although the convection-permitting climate simulations without the use of parameterization schemes have received great attention in recent years, little effort has been devoted to project future flood risks at a convection-permitting scale (horizontal grid spacing ≤4 km). Therefore, it is desired to project future changes in hydrologic regimes based on the convection-permitting climate simulations, improving robustness and reliability of flood risk projections (Prein et al., 2017; Qing et al., 2020; Wagner et al., 2013).

Floods typically result from the superposition of various physical processes and are commonly described by the peak, duration, and volume (Carvalho & Wang, 2019; Liu et al., 2018; Moftakhari et al., 2017). Previous univariate and bivariate flood risk assessments assume the missing flood characteristic to be the long-term, historical average and be independent of other characteristics considered, leading to overestimation or underestimation of flood risks (Alfieri et al., 2017; Balistrocchi et al., 2017). Thus, it is desired to explore the interdependence among flood characteristics, and multivariate approaches have received great attention in recent years (Brunner et al., 2019; Quinn et al., 2019; Santhosh & Srinivas, 2013). As one of the most popular multivariate approaches, copula has been extensively used to assess the dependence structure of flood characteristics and to estimate the return period of floods (Favre et al., 2004; Jeong et al., 2014; Mallakpour et al., 2019; Moftakhari et al., 2017). Since copulas applicable to a dimension of three or higher are limited, previous flood risk assessments are limited to two flood characteristics (e.g., the flood peak and volume), failing to obtain comprehensive risk assessments (Genest et al., 2007; Salvadori & De Michele, 2004; Salvadori et al., 2016; Serinaldi & Kilsby, 2013). Copula may also fail to accurately uncover the complex multidimensional dependence of flood characteristics, thereby leading to biased flood risk estimation (Daneshkhah et al., 2016; Liu et al., 2015). For example, a flood event with a high peak flow and large volume may occur with a long duration or a short duration, which depends on the dependence structure of flood characteristics. The misrepresentation of the dependence structure may lead to unreliable risk assessments on the prolonged contact with floodwaters.

Vine copula (also known as pair-copula construction), which is a more flexible approach than copulas, has been proven to be a powerful tool for describing the complex interactions of flood characteristics in a dimension of three or higher (Bedford & Cooke, 2002; Bevacqua et al., 2017; Daneshkhah et al., 2016; Jiang et al., 2019; Liu et al., 2018; Min & Czado, 2010; Yu et al., 2019). Previous vine copula studies commonly used local optimization schemes to estimate parameters, which is simple and computationally efficient to implement (Aas et al., 2009; Hobæk Haff & Segers, 2015; Sadegh et al., 2017). Such practice, however, may fail to achieve the global convergence of vine copula parameters, leading to a misrepresentation of the dependence structure of flood characteristics and thus biased risk assessments (Gruber & Czado, 2015, 2018). In addition, the vine copula simulation suffers from large uncertainty since the length of flood records is typically short. Little effort has been devoted to explicitly uncovering the underlying uncertainty in vine copula-based flood risk assessments (Daneshkhah et al., 2016; Dechant & Moradkhani, 2015; Farmer & Vogel, 2016; Ramos et al., 2013; Wang et al., 2018; Zhang et al., 2019). It is thus necessary to develop a robust vine copula approach for improving the reliability of flood risk assessment and for advancing our understanding of complex mechanisms and potential impacts of floods.

For the first time, we will develop probabilistic projections of multidimensional flood risks at a convection-permitting scale using the Weather Research and Forecasting (WRF) model and a Bayesian vine copula approach. The Markov chain Monte Carlo (MCMC) simulations will also be performed to address uncertainties in vine copula parameters and hydrological model parameters, leading to a probabilistic assessment of multidimensional flood risks. The Bayesian vine copula approach enables a robust assessment of the multidimensional dependence of flood characteristics including flood peak, volume, and duration. Future changes in flood episodes and associated return periods will be projected over Guadalupe and Mission river basins located in South Texas of the United States, which is the primary concern of the Texas Water Development Board and the Texas Department of Agriculture. The Parameter-elevation Regressions on Independent Slopes Model (PRISM) data set will be collected to verify the WRF simulations (Daly et al., 1994). The Model Parameter Estimation Experiment (MOPEX) data set (Duan et al., 2006) and the data collected from the United States Geological Survey (USGS) river flow gauging stations will be used to calibrate and validate hydrological simulations as well as to sample flood events.

The remainder of this study will be organized as follows. Section 2 will describe methods and data sets used in this study. Section 3 will present a flood risk assessment and underlying uncertainties, a high-resolution

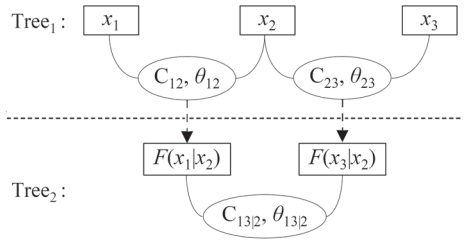

Figure 1. Schematic of a three-dimensional vine copula. x_1, x_2, and x_3 denote three interdependent random variables. C_{12}, C_{23}, and $C_{13|2}$ denote bivariate copulas with parameters θ_{12}, θ_{23}, and $\theta_{13|2}$, respectively. $F(x_1|x_2)$ and $F(x_3|x_2)$ denote conditional distribution functions.

projection of future changes in climate variables and runoff regimes, as well as an investigation of climate change impacts on multidimensional flood risks. Section 4 will provide uncertainty analysis of multidimensional flood risk assessment and hydrological nonstationarity assessment. Finally, conclusions and findings of this study will be drawn in Section 5.

2. Methods and Data Sources

2.1. Copula

Copulas are mathematical functions that can be used to derive the joint distribution of two or more random variables. Consider a vector $\boldsymbol{X} = (X_1,..., X_n)$ of random variables with a joint density function $f(x_1,..., x_n)$ and marginal cumulative distribution functions (CDFs) $F_1(x_1),..., F_n(x_n)$ as well as marginal probability density functions (pdfs) $f_1(x_1)$, ..., $f_n(x_n)$. According to Sklar's theorem (Sklar, 1959, pp. 229–231), the joint CDF $F(x_1, ..., x_n)$ can be expressed as

$$F\left(x_1,...,x_n\right) = C\left(F_1\left(x_1\right),...,F_n\left(x_n\right)\right) = C\left(u_1,...,u_n\right) \tag{1}$$

where C is a n-dimensional copula, that is, a joint CDF with uniform margins $(u_1, ..., u_n) \in [0, 1]^n$. The corresponding multivariate density can be decomposed as a product of the marginal distributions and the copula density

$$f\left(x_1,...,x_n\right) = f_1\left(x_1\right)\cdot\ldots\cdot f_n\left(x_n\right)\cdot c\left(u_1,\ldots,u_n\right) \tag{2}$$

where c is the copula density. Although the number of copula families applicable to a dimension of three or higher is limited, there exist tens of bivariate copula families for characterizing the dependence structure between two variables. This motivates pair-copula constructions (PCCs) for the flexible simulation of the high-dimensional dependence structure (Aas et al., 2009).

2.2. Bayesian Vine Copula Simulation of Flood Characteristics

Vine copula, also known as pair-copula construction (PCC), allows us to mathematically decompose an n-dimensional copula density into the product of $n(n-1)/2$ bivariate copulas. Such a decomposition enables a heterogeneous assignment of bivariate dependence types in a high-dimensional dependence structure, thereby yielding a robust simulation of flood characteristics. An n-dimensional vine is a nested set of trees, in which the edges of the tree i are the nodes of the tree $i + 1$ (for $i = 1, ..., n - 2$), and each tree has the maximum number of edges. A vine in which two edges in tree i are joined by an edge in tree $i + 1$ only if these edges share a common node, $i = 1, ..., n - 2$, is called regular vine. There are two special regular vines: the canonical vine (C-vine) and the D-vine, which are also the most widely used decompositions. A D-vine has no node connected to more than two edges, while each tree in a C-vine has a unique node connected to all other nodes. A three-dimensional regular vine is thus both a C- and a D-vine (Figure 1).

Assume that x_1, x_2, and x_3 in Figure 1 denote the flood peak (P), volume (V), and duration (D), respectively, which were identified in the form of runoff time series based on the Peaks over Threshold (POT) approach (Solari et al., 2017). The POT approach was selected since the annual maximum peak approach can include very low discharge values while missing peak values. Details of the POT-based flood event sampling are provided in supporting information S1. The joint density of the vine copula for the flood characteristics, $f(P, V, D)$, can be expressed as

$$\begin{aligned} f\left(P,V,D\right) = {} & f_P\left(P\right)\cdot f_V\left(V\right)\cdot f_D\left(D\right) \\ & \cdot c_{PV}\left\{F_P\left(P\right),F_V\left(V\right),\theta_{PV}\right\}\cdot c_{VD}\left\{F_V\left(V\right),F_D\left(D\right),\theta_{VD}\right\} \\ & \cdot c_{PD|V}\left\{F(P\mid V),F(D\mid V),\theta_{PD|V}\right\} \end{aligned} \tag{3}$$

Table 1
The Probability Distributions With the Highest Good-of-Fit for Flood Peak (P), Volume (V), and Duration (D) for Guadalupe and Mission River Basins, and the P-value for the Kolmogorov-Smirnov Test

River basin	Flood variable	Distribution	*p*-value
Guadalupe	Flood peak	Generalized Pareto	0.994
Guadalupe	Flood volume	Generalized extreme value	0.999
Guadalupe	Flood duration	Generalized extreme value	0.994
Mission	Flood peak	Generalized Pareto	0.995
Mission	Flood volume	Generalized Pareto	0. 999
Mission	Flood duration	Gumbel	0.995

where $f(\cdot)$ and $F(\cdot)$ denote the marginal pdf and CDF, respectively; c denotes the bivariate copula density; $(\theta_{PV}, \theta_{VD}, \theta_{PD|V})$ represents the pair-copula parameter set of which the number depends on the pair-copula family set; $F(P|V)$ and $F(D|V)$ denote the marginal conditional distributions that can be calculated using Equations 4 and 5, respectively, where C is the bivariate copula CDF (Joe, 1996). Equations 4 and 5 are also commonly defined as h-functions. More details of the vine copula model can be seen at Aas et al. (2009).

$$F(P \mid V) = h\left(P,V,\theta_{PV}\right) = \frac{\partial C_{PV}\left\{F_P\left(P\right),F_V\left(V\right),\theta_{PV}\right\}}{\partial F_V\left(V\right)} \tag{4}$$

$$F(D \mid V) = h\left(D,V,\theta_{VD}\right) = \frac{\partial C_{VD}\left\{F_D\left(D\right),F_V\left(V\right),\theta_{VD}\right\}}{\partial F_V\left(V\right)} \tag{5}$$

To identify the optimal marginal CDF for each flood characteristic, a total of 13 types of probability distributions were examined in this study, including Gaussian, gamma, exponential, Weibull, logistic, log-normal, log-logistic, Cauchy, Gumbel, generalized extreme value (GEV), generalized Pareto (GP), Pearson Type III, and inverse Gaussian. The optimal marginal CDF was determined using the Kolmogorov-Smirnov (K-S) test. The optimal marginal distribution fitting for each flood characteristic is shown in Figure S2 while the corresponding *P*-value for the K-S test is provided in Table 1.

There are two critical issues in constructing an appropriate vine copula model: vine structure specification and parameter estimation. A three-dimensional vine copula has three different structures, depending on the order of variables. The optimal structure can be simply selected based on the correlation measures between variables such as Kendall's τ. The parameter sets $(\theta_{PV}, \theta_{VD}, \theta_{PD|V})$ will be estimated using the MCMC simulation within a Bayesian framework, which simultaneously estimates the posterior distribution of all parameters in a vine copula model instead of the tree-by-tree deterministic estimation used in the frequentist vine copula approach. It should be noted that the parameter uncertainty in the marginal fitting is not included in the Bayesian vine copula but uncovered by a parametric bootstrap approach. The optimal pair-copula family set is selected from eight bivariate copula families, including Independence, Gaussian, Student t, Clayton, Gumbel, Frank, Joe, and BB1 based on the Akaike information criterion (AIC). The posterior distribution of the vine copula parameter vector $p(\theta_{PV}, \theta_{VD}, \theta_{PD|V}|P, V, D)$ given the flood characteristics, including the flood peak (P), volume (V), and duration (D), can be derived using a Bayesian formalism:

$$p(\theta_{PV},\theta_{VD},\theta_{PD|V} \mid P,V,D) = \frac{p\left(\theta_{PV},\theta_{VD},\theta_{PD|V}\right) \times p(P,V,D \mid \theta_{PV},\theta_{VD},\theta_{PD|V})}{p\left(P,V,D\right)} \tag{6}$$

where $p(\theta_{PV}, \theta_{VD}, \theta_{PD|V} \mid P, V, D)$ and $p(\theta_{PV}, \theta_{VD}, \theta_{PD \mid V})$ denote the posterior and prior distributions of vine copula parameters, respectively. $p(P, V, D \mid \theta_{PV}, \theta_{VD}, \theta_{PD \mid V}) \cong L(\theta_{PV}, \theta_{VD}, \theta_{PD|V} \mid P, V, D)$ denotes the likelihood function; $p(P, V, D)$ denotes the evidence that acts as a normalization constant, which can be excluded from the Bayesian analysis in practice. Thus, the formulation of Equation 6 can be simplified as

$$p(\theta_{PV},\theta_{VD},\theta_{PD|V} \mid P,V,D) = p\left(\theta_{PV},\theta_{VD},\theta_{PD|V}\right) \times L(\theta_{PV},\theta_{VD},\theta_{PD|V} \mid P,V,D) \tag{7}$$

The likelihood function $L(\cdot|\cdot)$ is usually given by the sum of all logarithmically transformed bivariate copula densities in a vine copula (Equation 8) for simplicity and numerical stability, where $u_P = F_P(P)$; $u_V = F_V(V)$; $u_D = F_D(D)$. It should also be noted that the frequentist vine copula approach also uses Equation 8 as the likelihood function but uses local optimization algorithms (e.g., the L_BFGS-B method) to sequentially estimate parameters (Nagler et al., 2019)

$$\ell\left(\theta_{PV},\theta_{VD},\theta_{PD|V} \mid u_P,u_V,u_D\right) = \sum_{t=1}^{T}\log\left\{c_{PV}\left(u_{P,t},u_{V,t},\theta_{PV}\right)\right\} + \sum_{t=1}^{T}\log\left\{c_{VD}\left(u_{V,t},u_{D,t},\theta_{VD}\right)\right\} + \sum_{t=1}^{T}\log\left\{c_{PD|V}\left(u_{P|V,t},u_{D|V,t},\theta_{PD|V}\right)\right\} \quad (8)$$

The prior distribution is drawn using the Latin Hypercube Sampling (LHS) technique, which may not be the optimal sampler yet the relatively efficient one and has been used in numerous studies for implementing robust MCMC simulations (Huang et al., 2018; McKay et al., 1979; Vrugt, 2016).

When the prior distributions are specified, the posterior distributions of vine copula parameters can be estimated by the repeated Monte Carlo sampling in the prior parameter space. Specifically, the MCMC simulation begins at drawing *LN* samples from the entire prior space, $p(\theta_{PV}, \theta_{VD}, \theta_{PD|V})$, using LHS, and each sample is given by a d-dimensional vector $(\theta_{PV}, \theta_{VD}, \theta_{PD|V})$ (Note that d is not necessarily three since the number of parameters for some bivariate copula families is >1). The *LN* samples are randomly assigned to N complexes, and the sample with the highest log-likelihood value, $\ell(\cdot \mid \cdot)$, is selected as the starting point for each Markov chain. During the algorithm progression, adaptive metropolis (AM) and differential evolution (DE) algorithms are used for different chains to create the proposal point z_p (Sadegh et al., 2017), and the acceptance or rejection of proposal is determined through calculating the Metropolis acceptance probability

$$p_{\text{accept}}\left(z_c \rightarrow z_p\right) = \min\left[1, \frac{p\left(z_p\right)}{p\left(z_c\right)}\right] \quad (9)$$

where z_c denotes the current point; $p(z_c)$ and $p(z_p)$ denote the probability density of the current point and the candidate point, respectively. Such an acceptance/rejection rule enables the sequential update of the Markov chains and thus the convergence to the posterior distribution. The multichain $\hat{R}$ diagnostic of Gelman and Rubin (1992) was used in this study to estimate the convergence of the MCMC simulation. A $\hat{R}$-statistic value below 1.2 means that the MCMC convergence is achieved (Vrugt, 2016). It should be noted that the MCMC simulation mentioned above is not limited to the inference of the three-dimensional vine copula and can be applicable to a higher dimension.

2.3. Convection-Permitting Projection of Multidimensional Flood Risks

To generate high-resolution climate information for flood risk projections, the WRF model v3.7.1 was employed to conduct the convection-permitting climate simulations over Texas (Figure 2a). The model was operated at a region of 1,520 × 1,400 km (380 × 350 grid points) with 51 stretched vertical levels topped at 50 hPa. The model domain has a 4-km horizontal grid spacing, which is fine enough to resolve convective processes and well capture the details of the complex terrain. Thus, convection parameterization is not required for performing the 4 km WRF simulations. The initial and lateral boundary conditions of the WRF simulation are provided by the NCEP Climate Forecast System Reanalysis (CFSR) data set with a 6-h temporal resolution and a 0.5° × 0.5° spatial resolution. The model was configured using the Rapid Radiative Transfer Model shortwave and longwave radiation scheme, the revised Monin-Obukhov surface layer scheme, the Yonsei University (YSU) planetary boundary layer scheme, as well as the Tompson cloud microphysics scheme. The Noah-MP land surface scheme was used to simulate the land surface. The PRISM data set was collected to evaluate the reliability of the WRF simulations.

The WRF runs were carried out during 1981–1995 for historical simulations and 2085–2099 for future projections. The future projections were forced with the CFSR data consecutively perturbed using the Pseudo-Global Warming (PGW) technique (Lauer et al., 2013; Wang & Wang, 2019), since previous studies have demonstrated the high potential of the PGW approach to satisfactorily downscale future climates (Hara et al., 2008; Yoshikane et al., 2012). Although the use of the PGW approach with the GCM ensembles can barely address the interaction between the large-scale climate system beyond the model boundary and local weather, it not only reduces large-scale model biases but also requires fewer computational resources than a continuous simulation spanning a century. Such advantages are especially important for

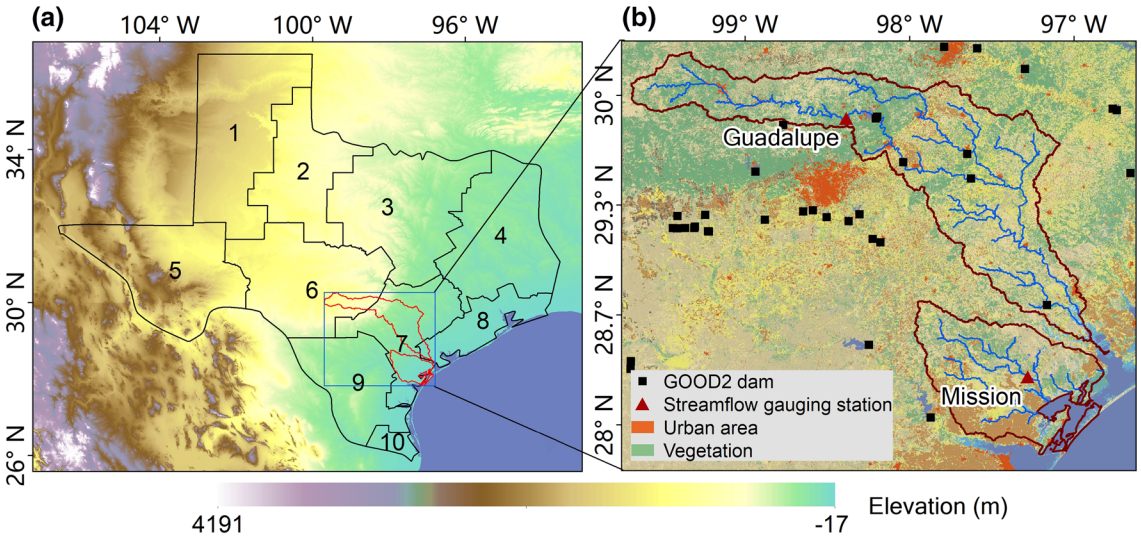

Figure 2. (a) Model domain with topography and Texas climate divisions including: (1) High Plains; (2) Low Rolling Plains; (3) North Central Texas; (4) East Texas; (5) Trans Pecos; (6) Edwards Plateau; (7) South Central Texas; (8) Upper Coast; (9) South Texas; (10) Lower Valley. (b) Guadalupe and Mission river basins over South Texas with land use. The red triangles represent the location of the United States Geological Survey gauging stations, and the black squares represent the location of dams collected from the Global Georeferenced Database of Dams (GOOD2) (Mulligan et al., 2020).

the convection-permitting simulation that is extremely computationally expensive. The perturbed physical fields include surface variables (e.g., sea level pressure, soil temperature, and sea surface temperature) and three-dimensional field variables (e.g., specific humidity, temperature, geopotential height, as well as the eastward and northward components of horizontal wind). Note that sea ice was not perturbed in this study because sea ice does not exist in the model domain. A 30-year ensemble of 15 GCMs from the Coupled Model Intercomparison Project Phase 5 (CMIP5) with a high emission scenario (RCP8.5) was collected to calculate the mean climate change signal and thus estimate the climate perturbation (Equation 10). The 15 GCMs were selected based on their performance in simulating the climate over North America and their details are provided in Table S1. RCP8.5 is a scenario of comparatively high greenhouse gas emissions with stabilizing near 8.5 W/m^2(Moss et al., 2010)

$$\mathrm{WRF}_{\mathrm{input}} = \mathrm{CFSR} + \left(\mathrm{CMIP5}_{2071-2100} - \mathrm{CMIP5}_{1976-2005}\right) \tag{10}$$

After deriving the climate change signal, the perturbation of the CFSR reanalysis data was conducted every 6 h in order to provide the WRF model with initial and boundary conditions for future climate projections.

Although there is a sophisticated coupling architecture (i.e., WRF-Hydro) widely used for coupling of hydrological models with the WRF climate simulations, previous studies have demonstrated that the WRF-Hydro-simulated streamflow tends to have large biases over South Texas (Lin et al., 2018a, 2018b; Salas et al., 2018). To examine the impact of climate change on flood risk, daily streamflow in the Guadalupe and Mission river basins (Figure 2b) was predicted using the rainfall-runoff model (Hymod) forced by precipitation and potential evapotranspiration (PET) projected from the convection-permitting WRF climate simulations. The performance of the Hymod in streamflow simulation over South Texas has been verified in previous studies (Herman et al., 2013; Roy et al., 2017; Vrugt et al., 2008; Wang et al., 2018). Given the absence of the PET observation, the FAO-56 Penman-Monteith Equation was used to calculate the PET as an alternative (Allen et al., 1998). The Hymod is a well-known rainfall-runoff model with five parameters $C_{\max}$, $b_{\exp}$, β, R_s, and R_q. The detailed description on the five parameters is provided in Table S2. As it is not likely to measure model parameters directly, an initial uncertainty range was usually given for each parameter (see Table S2). In addition, the inherent uncertainty in hydrologic model parameters was addressed through the MCMC simulation. The difference between the MCMC-based vine copula inference and the MCMC-based hydrological prediction is the likelihood function used in this study. Assume that $\tilde{Y}$ and θ_h signify a discrete vector of discharge obser-

vations and Hymod parameters, respectively, the log-likelihood function in the MCMC-based hydrological prediction can be formalized as Equation 11

$$\ell\left(\theta_{\mathrm{h}} \mid \tilde{Y}\right) = -\frac{n}{2}\ln\left(2\pi\right) - \frac{n}{2}\ln\tilde{\sigma}^2 - \frac{1}{2}\sum_{t=1}^{n}\left(\frac{\tilde{y}_t - y_t\left(\theta_{\mathrm{h}}\right)}{\tilde{\sigma}}\right)^2 \tag{11}$$

where $\tilde{Y}_t$ is the discharge observation at time t and $y_t(\theta_{\mathrm{h}})$ is the corresponding simulation given parameter θ_{h} at time t; $\tilde{\sigma}$ is the estimated standard deviation of the measurement error. The MOPEX data set and the USGS streamflow observation were used to calibrate and validate hydrological simulations. The MCMC simulation generates the posterior distribution of model parameters, leading to a probabilistic streamflow prediction with uncertainty intervals.

The multidimensional dependence of the POT-based historical flood characteristics including the flood peak (P), volume (V), and duration (D) was simulated by the Bayesian vine copula in Section 2.2. The future flood events can be sampled from the projected streamflow time series through the procedure described in supporting information S1, and thus the associated return period of each flood event can be derived through the constructed Bayesian vine copula. Two widely used cases of flood return period are "AND" and "OR" cases, also known as primary return periods (Salvadori & De Michele, 2004). The trivariate return period of "OR" case (T_{OR}) corresponds to that at least one of the flood peak (P), volume (V), and duration (D) exceeds their respective thresholds p^*, v^*, and d^*, while the "AND" case (T_{AND}) corresponds to that the three flood variables exceed their respective thresholds simultaneously. T_{OR} and T_{AND} can be defined as Equations 12 and 13, respectively

$$\begin{aligned} T_{OR} &= \frac{\mu}{\Pr\left(P \geq p^*, \vee V \geq v^*, \vee D \geq d^*\right)} = \frac{\mu}{1 - \Pr\left(P \leq p^*, V \leq v^*, D \leq d^*\right)} \\ &= \frac{\mu}{1 - C\left(u_{p^*}, u_{v^*}, u_{d^*}, \hat{\theta}_{PV}, \hat{\theta}_{VD}, \hat{\theta}_{PD|V}\right)} \end{aligned} \tag{12}$$

$$\begin{aligned} T_{AND} = \frac{\mu}{\Pr\left(P \geq p^*, V \geq v^*, D \geq d^*\right)} &= \frac{\mu}{1 - \Pr\left(P \leq p^*\right) - \Pr\left(V \leq v^*\right) - \Pr\left(D \leq d^*\right) +} \\ &\quad \Pr\left(P \leq p^*, V \leq v^*\right) + \Pr\left(P \leq p^*, D \leq d^*\right) + \\ &\quad \Pr\left(V \leq v^*, D \leq d^*\right) - \Pr\left(P \leq p^*, V \leq v^*, D \leq d^*\right) \\ &= \frac{\mu}{1 - u_{p^*} - u_{v^*} - u_{d^*} + C_{PV}\left(u_{p^*}, u_{v^*}, \hat{\theta}_{PV}\right) + C_{VD}\left(u_{v^*}, u_{d^*}, \hat{\theta}_{VD}\right) +} \\ &\quad C_{PD}\left(u_{p^*}, u_{d^*}, \hat{\theta}_{PD}\right) - C\left(u_{p^*}, u_{v^*}, u_{d^*}, \hat{\theta}_{PV}, \hat{\theta}_{VD}, \hat{\theta}_{PD|V}\right) \end{aligned} \tag{13}$$

where $u_{p^*} = F_P(p^*)$; $u_{v^*} = F_V(v^*)$; $u_{d^*} = F_D(d^*)$; μ denotes the average interarrival time between the occurrences of flood events. The return period is not deterministic but probabilistic with uncertainty intervals as a result of three sources of uncertainty, including hydrological simulations, marginal distributions, and vine copula parameters derived from the MCMC simulation in Section 2.2. It should be noted that the multivariate return period of hydrological loads does not generally correspond to that of structure failure. However, the likelihood of failure in water infrastructure is expected to increase due to more frequent exposure to extreme events (Mallakpour et al., 2019). Thus, the possible changes in the return period of flood episodes provide meaningful insights into the maintenance and modification of aged water infrastructure to improve

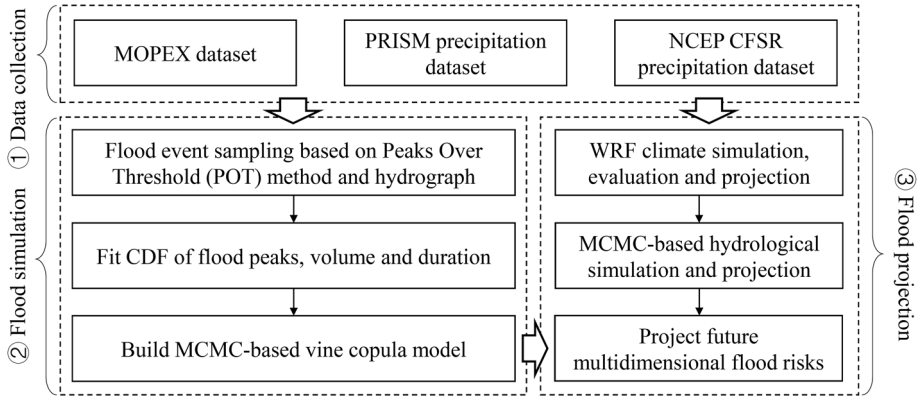

Figure 3. Flowchart of the convection-permitting projections of multidimensional flood risks. CDF, cumulative distribution function; CFSR, Climate Forecast System Reanalysis; MCMC, Markov chain Monte Carlo; MOPEX, Model Parameter Estimation Experiment; NCEP, National Centers for Environmental Prediction; PRISM, Parameter-elevation Regressions on Independent Slopes Model; WRF, Weather Research and Forecasting.

adaptation and resilience to the intensification of flood risk in a changing climate. Detailed steps of the convection-permitting flood risk projections are illustrated in Figure 3.

2.4. Data Sources

The PRISM data set, a gridded data set with a 4 × 4 km grid resolution, was collected to evaluate the performance of the WRF simulation over Texas (Daly et al., 1994). The MOPEX data set (including daily precipitation, PET, and streamflow) during 1981–1995 was also collected to calibrate and validate hydrological simulations over Guadalupe and Mission river basins (Duan et al., 2006). The Guadalupe river basin is one of the three most dangerous regions in the United States for flash floods (Guadalupe-Blaco River Authority, n.d.), while the Mission river basin is also one of the most susceptible to flooding in Texas (TFMA, 2015). The hydrologic simulation was calibrated based on the MOPEX data set during 1981–1990 and then validated during 1991–1995. The Guadalupe river basin has a subtropical, humid climate characterized by hot summers and mild winters with a contributing drainage area of 1,315 square miles. The Mission river basin has a subtropical, humid climate characterized by hot, humid summers and generally mild to cool winters with a contributing drainage area of 690 square miles. Both of the two USGS gauging stations are far away from dams (see Figure 2b), thereby reducing the impacts of human regulation on flood risk projections. The USGS daily mean streamflow observation during 1948–2017 was collected to conduct flood event sampling and thus to construct Bayesian vine copula as well as to project future flood risk in a changing climate. Therefore, flood risks were essentially assessed on a 70-year temporal scale although climate change impacts on flood risks were assessed based on flood events for 15 years.

For the future projection of flood risks, the daily streamflow during 2085–2099 was predicted based on the projected future changes in precipitation and PET. The future flood events were sampled based on the flood peak threshold estimated by the approach introduced in supporting information S1. The return period of each future flood event was then calculated using the Bayesian vine copula constructed based on flood events identified during 1948–2017.

3. Results Analysis

3.1. Probabilistic Flood Simulation Using Bayesian Vine Copula

The flood characteristics, including the peak, volume, and duration, were identified by the POT approach described in supporting information S1 to perform multidimensional flood frequency analysis, leading to the optimal flood peak thresholds of 3,290 and 3,090 ft^3/s for Guadalupe and Mission river basins, respective-

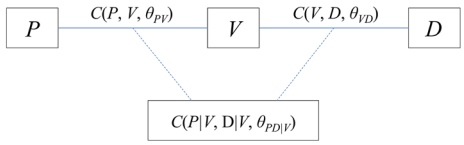

Figure 4. Selected vine structure for the flood samples with three variables, including flood peak (P), volume (V), and duration (D).

ly. This leads to 98 and 101 flood peaks, respectively, during 1948–2017. The corresponding flood volume and duration are identified through the generated hydrographs. The detailed flood peak threshold selection was illustrated in Figure S1.

To perform the probabilistic simulation of flood variables including the flood peak (P), volume (V), and duration (D), the vine copula structure is determined based on the correlation measure between flood variables, chi-plots, and Kendall's plots. Both of the chi-plots and Kendall's plots of the paired flood variables indicate a positive dependence between the pairwise flood variables for Guadalupe and Mission river basins while the degree of dependence between P and D is relatively low (see Figure S3). Such a difference can also be revealed by the correlation measures. For example, for the Guadalupe river basin, the Pearson's correlation coefficients for (P, V), (V, D), and (P, D) are 0.79, 0.73, and 0.33, respectively; the corresponding values for the Mission river basin are 0.93, 0.39, and 0.22, respectively. Therefore, the flood variable V should be placed between the other two variables as illustrated in Figure 4.

After determining the vine structure, the MCMC simulation was conducted to estimate the posterior distributions of vine copula parameters. Figure 5 presents the convergence of the MCMC chains to the posterior distribution, which is achieved within <1,000 iterations where the $\hat{R}$ values drop below the critical threshold of 1.2 for all parameters. The selected pair-copula family sets for Guadalupe and Mission river basins are (Gumbel, BB1, and Gaussian) and (Frank, Gumbel, Frank), respectively. Compared to the frequentist vine copula approach, the Bayesian vine copula leads to different pair-copula family sets with lower AIC values (see Table 2), indicating a better characterization of the dependence structure of flood variables. Such an improvement can be due to the fact that the frequentist vine copula approach estimates pair-copula parameters sequentially starting from the top tree by using local algorithms, thereby often getting trapped in local minima. The posterior distributions of the vine copula parameters derived by the MCMC simulation are shown in Figure 6. Figure 6 also presents the Maximum A Posteriori (MAP) parameter values, indicated by red asterisks. It can be seen that large uncertainty exists in the vine copula parameters, especially for the Mission river basin. The goodness of fit of pair copulas was evaluated using the two-sample Cramér-von Mises test (see Table 3). A higher P-value indicates a greater confidence in the fit of pair copulas. Overall, the fitting of pair copulas is plausible, indicating reasonable simulations on the complex dependence structure of flood variables. Therefore, the Bayesian vine copula approach retains a desirable feature as it not only correctly identifies the maximum likelihood estimates but also samples the underlying probability distribution of parameter sets that are equally good at reproducing the dependence structure. Such a feature provides multiple plausible scenarios of multidimensional flood characterization, leading to a probabilistic flood risk assessment with uncertainty information.

To further uncover the uncertainty of vine copula parameters, the "OR" and "AND" case hydrological design point (p, v, d) for the return period of 10 years were estimated using the Bayesian vine copula (Salvadori & De Michele, 2004; Salvadori et al., 2016). Details of the trivariate hydrologic design estimation are provided in supporting information S2. Figure 7 depicts 30 scenarios of design peak and volume (black points) for a return period of 10 years including the "OR" case (a and c) and the "AND" case (b and d) for Guadalupe (a and b) and Mission (c and d) river basins. The 30 scenarios of design values result from 30 different parameter sets extracted from the posterior distribution as shown in Figure 6. It is noteworthy that the design

Table 2
The Optimal Pair-Copula Family Set and Akaike Information Criterion (AIC) Based on Bayesian Vine Copula and Sequential Vine Copula

River basin	Approach	Pair-copula family	AIC
Guadalupe	Bayesian vine copula	Gumbel, BB1, and Gaussian	−249
Guadalupe	Sequential vine copula	Gaussian, BB1, and Frank	−245
Mission	Bayesian vine copula	Frank, Gumbel, Frank	−218
Mission	Sequential vine copula	Joe, BB1, Frank	−214

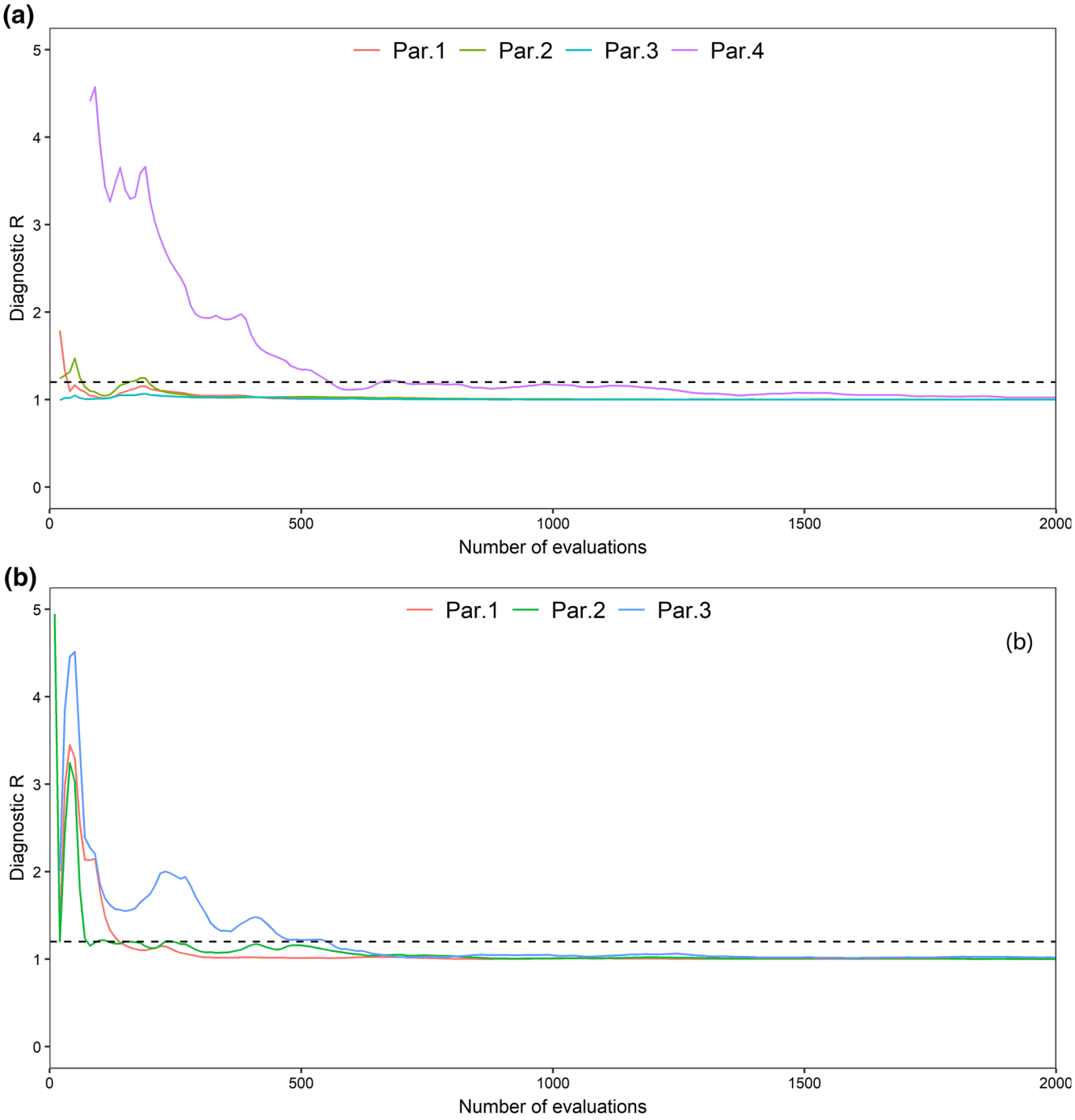

Figure 5. Evolution of the convergence diagnostic $\hat{R}$ values for the MCMC simulation for Guadalupe (a) and Mission (b) river basins. The $\hat{R}$ values of different parameters are depicted with colored lines. The convergence to the posterior parameter distribution is achieved if the lines consistently fall below a value of 1.2 (the dashed line). Note that the number of parameters in (a and b) is different since the optimal bivariate copula families are different. MCMC, Markov chain Monte Carlo.

flood duration is obtained in the trivariate vine copula but is not shown in Figure 7 for better visualization. The red points are the corresponding design points estimated using the frequentist vine copula approach. The uncertainty in the marginal fitting uncovered by the parametric bootstrap approach is also shown in Figure 7, as indicated by the gray lines. Results indicate that there is a good agreement between the frequentist deterministic approach and the Bayesian approach for estimating design variables. The frequentist

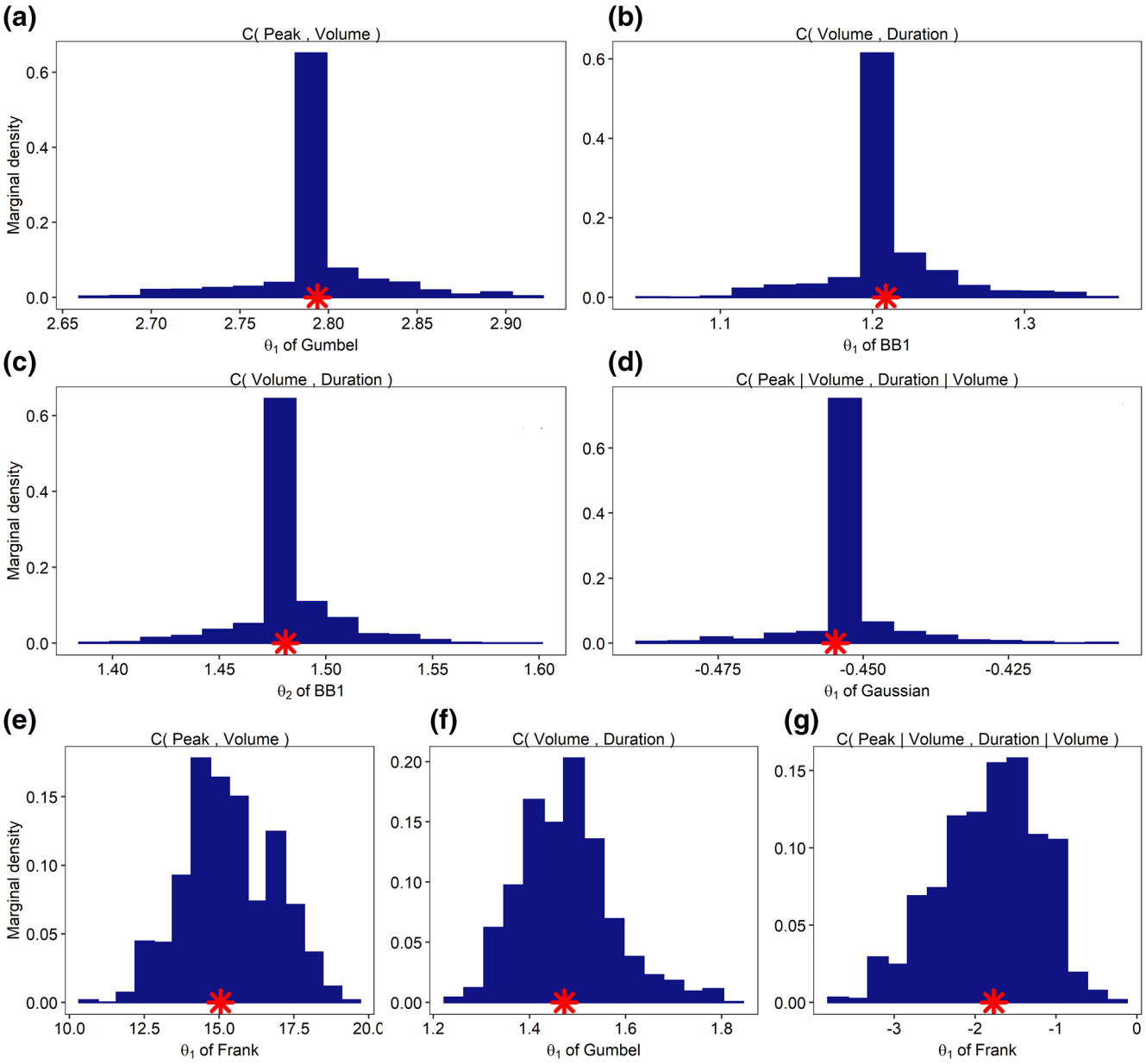

Figure 6. Posterior distributions of the three-dimensional vine copula parameters for Guadalupe (a–d) and Mission (e–g) river basins. Gumbel, BB1, Frank, and Gaussian are bivariate copula families. The red asterisks show the Maximum A Posterior (MAP) parameter values. Note that the BB1 copula has two parameters while Gumbel and Frank have one parameter.

approach, however, neglects the other acceptable design estimates with an equally high probability, posing a potential risk to the design of hydrological infrastructures. For example, as shown in Figure 7c, the design peak and volume estimated using the frequentist approach (the red point) are 43,920 and 117,930 ft^3, respectively; however, the largest design peak and volume among the 30 scenarios are 54,217 and 131,060 ft^3, respectively. Such a large uncertainty deserves more attention for a reliable hydrologic design using the vine copula in future studies. In addition, Figure 7 depicts the relative contribution of uncertainties in copula parameters and the marginal fitting. The marginal uncertainty, denoted by the gray lines, is larger than the uncertainty in the vine copula parameters, represented by the black scatter points.

Table 3
The Two-Sample Cramér-von Mises Test for Pair Copulas in the Trivariate Vine Copulas for Guadalupe and Mission River Basins

River basin	Pair copulas	Copula family	MAP parameter value	*p*-value
Guadalupe	$C(P, V)$	Gumbel	$\theta = 2.79$	0.905
Guadalupe	$C(V, D)$	BB1	$\theta_1 = 1.21, \theta_2 = 1.48$	0.998
Guadalupe	$C(P\|V, V\|D)$	Gaussian	$\theta = -0.45$	0.556
Mission	$C(P, V)$	Frank	$\theta = 15.32$	0.949
Mission	$C(V, D)$	Gumbel	$\theta = 1.46$	0.937
Mission	$C(P\|V, V\|D)$	Frank	$\theta = -1.75$	0.203

Note. P, V, and D denote flood peak, volume, and duration, respectively. The pair-copula families and corresponding Maximum A Posteriori (MAP) parameter values are estimated using the Bayesian vine copula.

3.2. Evaluation of Convection-Permitting Climate Simulation

To assess climate change impacts on flood risks, the performance of the convection-permitting WRF climate simulation was evaluated using the PRISM data set. Figure 8 shows the spatial distributions of the 15-year annual, summer (June-July-August, JJA) and winter (December-January-February, DJF) mean precipitation derived from the WRF simulation and the PRISM data set, as well as the corresponding absolute biases. In general, the WRF simulation and the PRISM data set show a similar spatial pattern of the annual and seasonal mean precipitation. The WRF simulation tends to overpredict the annual mean precipitation over Southeast Texas while it has an underestimation over Northwest Texas, as shown in Figure 8c. In addition, there is a remarkable variation of the absolute biases between summer (Figure 8i) and winter (Figure 8f). The winter mean precipitation derived from the WRF simulation and the PRISM data set shows an excellent agreement over most areas of Texas except East Texas. In comparison, the WRF-simulated summer mean precipitation tends to have a dry bias of <80 mm/year over South Texas while it has a wet bias over the northern domain.

To further evaluate the performance of the WRF-simulated precipitation, the Taylor Diagram was used to depict how closely the patterns from the WRF simulation and the CFSR data set match the PRISM observation. The Taylor Diagram presents the correlation coefficient (COR), standard deviation (SD), and root-mean-square-error (RMSE) between the simulated precipitation and the observed precipitation in a graphical way. The simulated pattern agrees better with observations if the model has a higher correlation and a more consistent standard deviation with the observation, as well as it lies nearer the point marked "OBS" on the x-axis. Figure 9 presents the relative merits of WRF and CFSR with respect to reproducing the spatial patterns of daily mean precipitation over 10 climate divisions of Texas. Most CFSR data sets have high CORs between 0.6 and 0.9 except for Upper Coast (division 8) and Lower Valley (division 10). In comparison, all the WRF simulations have higher CORs than the CFSR data set for each climate division. The WRF simulation also has more consistent SDs with the PRISM observation compared to the CFSR data set. For example, all the WRF-simulated patterns have SDs between 1 and 1.2; in comparison, multiple CFSR patterns have SDs <0.8. These findings reveal that the WRF simulation has a relatively high skill of reproducing the spatial distribution of daily mean precipitation over Texas compared to the CFSR data set. Such an improvement can be attributed to the explicit resolution of the convection processes and the detailed characterization of the fine-scale spatial heterogeneity in the WRF simulation, which cannot be characterized by the CFSR product with a relatively coarse spatial resolution.

In addition to the long-term mean precipitation analysis, the WRF-simulated extreme precipitation was evaluated against the PRISM observation at a daily timescale using three indices including very wet days (R95Ptot), maximum 1-day precipitation (Rx1day), and number of very heavy precipitation days (R20mm). Definition of these indices is provided in Table 4. The spatial distributions of the 15 year mean precipitation extremes generated from the PRISM observation and the WRF simulation are depicted in Figure 10. In general, the WRF simulation well reproduces the spatial pattern of all the three precipitation indices although it shows overprediction over certain regions. Specifically, the WRF simulation tends to overpredict the three precipitation extremes in the western mountainous region. In comparison, the consistency between the WRF-simulated and observed extremes is relatively high in the eastern region. Among the three extreme indices, the WRF-simulated R20mm is the most consistent with the PRISM observation over South and East Texas with slight model biases. To further assess the skill of WRF in simulating the intensity and frequency of precipitation events, the histograms of daily precipitation from the PRISM observation and the WRF simulation are also examined for 10 climate divisions of Texas (see Figure 11). In general, the WRF simulation is able to accurately reproduce the daily precipitation distribution for all climate divisions. Although the frequency of light precipitation events is overpredicted, the WRF-simulated intense precipitation events (>30 mm/day) have consistent frequencies with the PRISM observation. Therefore, the WRF simulation

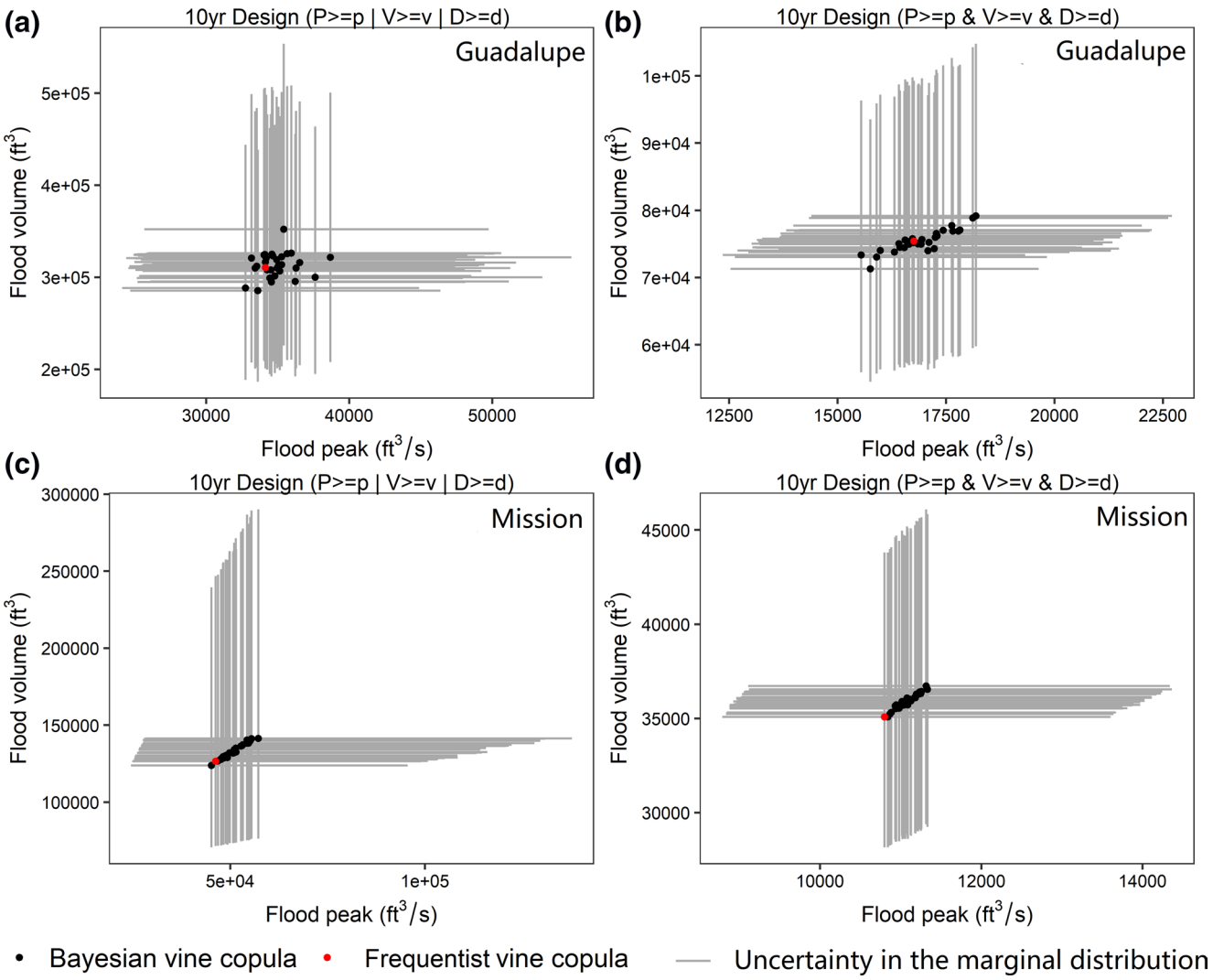

Figure 7. Multiple scenarios of hydrological design variables including flood peak and volume for a design return period of 10 years derived by the Bayesian vine copula for Guadalupe and Mission river basins. Panels (a and c) represent the return period of "OR" case while panels (b and d) represent the "AND" case. The black scatter points represent 30 scenarios of the design values resulting from the posterior distributions of vine copula parameters while the red points represent the design value derived using the frequentist vine copula approach. The gray lines represent the uncertainty in the marginal fitting derived using the parametric bootstrap approach.

illustrates its ability to reproduce the observed short-term extreme precipitation even though discrepancies exist, which ensures credibility of flood risk projection.

3.3. Probabilistic Rainfall-Runoff Prediction

To assess the climate-induced flood risks at a convection-permitting scale, probabilistic hydrological simulations were conducted to predict streamflow regimes for Guadalupe and Mission river basins. The MCMC simulation was used to explicitly address the parameter uncertainty in hydrological simulations. The daily streamflow observation during 1981–1990 was used to calibrate the hydrological simulation. The posterior distributions of hydrologic model parameters for Guadalupe (a–e) and Mission (f–j) river basins are shown in Figure S4. The parameter posterior distributions were used to predict daily streamflow during 1991–1995, which was then compared against the streamflow observation from the MOPEX data set. Figure 12 depicts the daily streamflow simulations with the 95% uncertainty range for model calibration (1981–1990) and validation (1991–1995) over Guadalupe (a) and Mission (b) river basins. Results indicate

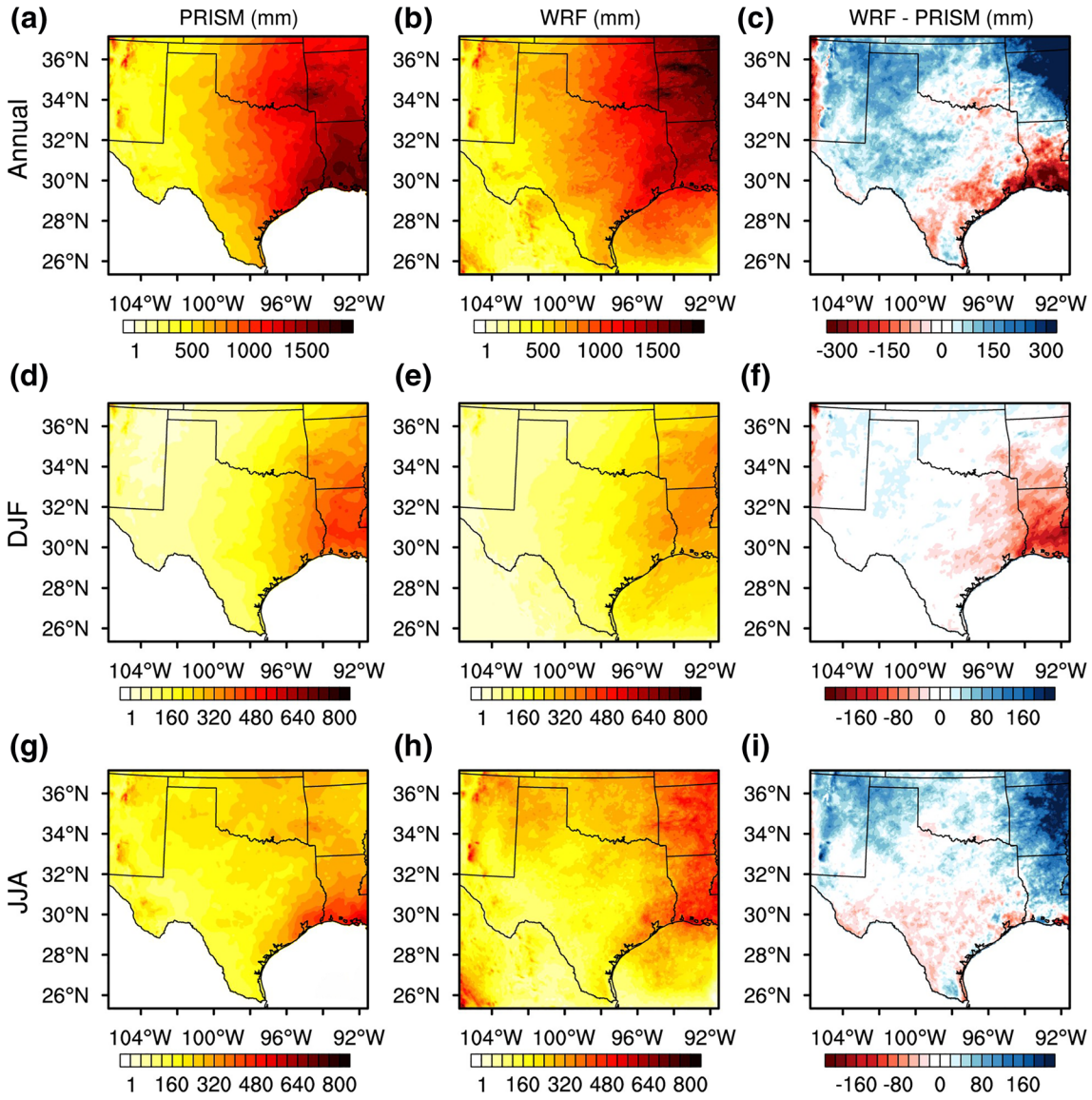

Figure 8. Spatial patterns of 15-year mean precipitation generated from the PRISM observation, the WRF simulation, and absolute model bias (WRF-PRISM). (a–c) Annual, (d–f) DJF, and (g–i) DJF. DJF, December-January-February; JJA, June-July-August; PRISM, Parameter-elevation Regressions on Independent Slopes Model; WRF, Weather Research and Forecasting.

that 87.55% and 90.15% of the observed streamflow fall within the 95% uncertainty range in the calibration period for Guadalupe and Mission river basins, respectively. 87.81% and 85.84% of streamflow observations are captured in the validation period for Guadalupe and Mission river basins, respectively. Such a substantial proportion of observations captured by probabilistic simulations indicates that the hydrological simulation well characterizes the rainfall-runoff behavior in the Guadalupe and Mission river basins.

As precipitation is the most important driving factor for predicting hydrological regimes and flood risks, the absolute and relative difference of the 15-year annual and seasonal mean precipitation between past and future climates are shown in Figure 13. A significant drying tendency is observed at the northeastern corner of the model domain, with a considerable reduction of 300 mm/year in the amount of precipitation (Figure 13a). In addition, certain areas are projected to become wetter especially for the Gulf Coast with an increased precipitation of nearly 200 mm/year. The increase and decrease of annual precip-

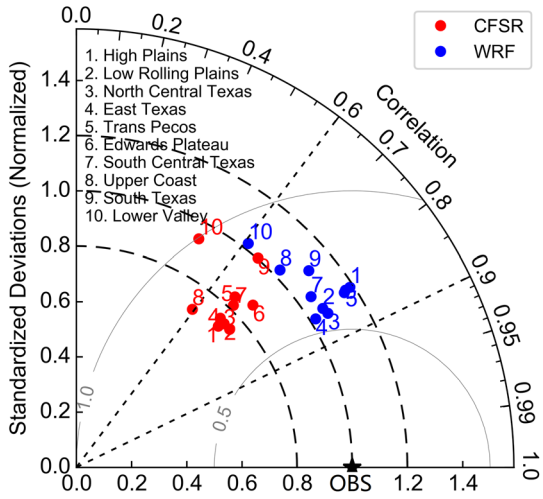

Figure 9. Comparison of daily mean precipitation from the WRF simulation and the CFSR data set during 1981–1995 over 10 climate divisions of Texas. CFSR, Climate Forecast System Reanalysis; WRF, Weather Research and Forecasting.

itation, however, are generally <25% compared to the historical annual precipitation (Figure 13b). Figures 13c and 13d show a general increase of the winter precipitation except for the Gulf of Mexico and the eastern Mexico. Compared to the winter precipitation, the summer precipitation shows a more significant change between the past and future climates. For example, Figure 13e shows a large reduction in precipitation of up to 160 mm at the northeastern corner of the domain. In contrast, the Gulf Coast and the boundary between Texas and Mexico show a significant wetting, with an increase of 160 mm in the amount of precipitation.

To examine extreme precipitation changes in a warming climate, Figure 14 presents the absolute and relative difference of the 15-year mean precipitation extremes between past and future climates. The changes in the three extreme precipitation indices show different patterns in a warming climate, but all of them are projected to increase over South Texas, indicating the increasing risk of flooding over our study area. For example, the maximum one-day precipitation (Rx1day) is projected to increase by up to 54% in most areas of Texas, indicating the significant increase in the frequency of extreme precipitation and thus more frequent occurrences of flash floods.

The calibrated hydrologic model forced by the projected daily precipitation generates the probabilistic prediction of future streamflow time series, as shown in Figure 15. The proportion of rainy days during the 15 years decreases from 63% to 55% and from 59% to 57% for Guadalupe and Mission river basins, respectively. However, the frequency of extreme precipitation has largely increased for both river basins. For example, Guadalupe and Mission river basins have, respectively, experienced 98 and 103 heavy rainfall events with daily precipitation over 25 mm during 1981–1995, and the mean precipitation for these events are 39 and 42 mm; in comparison, the two river basins are projected to experience 131 and 171 such heavy rainfall events in the future with the mean precipitation of 46 and 56 mm, respectively. The total precipitation amount of the heaviest rainfall event is also projected to increases from 99 to 160 and from 188 to 310 mm for Guadalupe and Mission river basins, respectively. These findings indicate that a large increase in the frequency and intensity of extreme precipitation is projected to occur in a changing climate, whereas the number of rainfall events is expected to decrease over South Texas. And the increase of the extreme precipitation over the Mission river basin is relatively larger than the Guadalupe river basin. It should be noted that such an intensification of extreme precipitation is projected under a high emissions pathway (RCP8.5), which would vary under different emissions pathways. The future changes in extreme precipitation are expected to affect flood risks in a changing climate, which will be assessed through the constructed Bayesian vine copula.

Table 4
Extreme Precipitation Indices Used in This Study

Index label	Name	Definition	Unit
R95pTOT	Very wet days	Total precipitation of wet days with daily precipitation exceeding the 95th percentile of the daily precipitation at wet days	mm
Rx1day	Maximum one-day precipitation	Highest precipitation amount in 1-day period	mm
R20mm	Number of very heavy precipitation days	Annual count of days with daily precipitation exceeding 20 mm	Days

Note: A "wet day" is a day with at least 1.0 mm of precipitation.

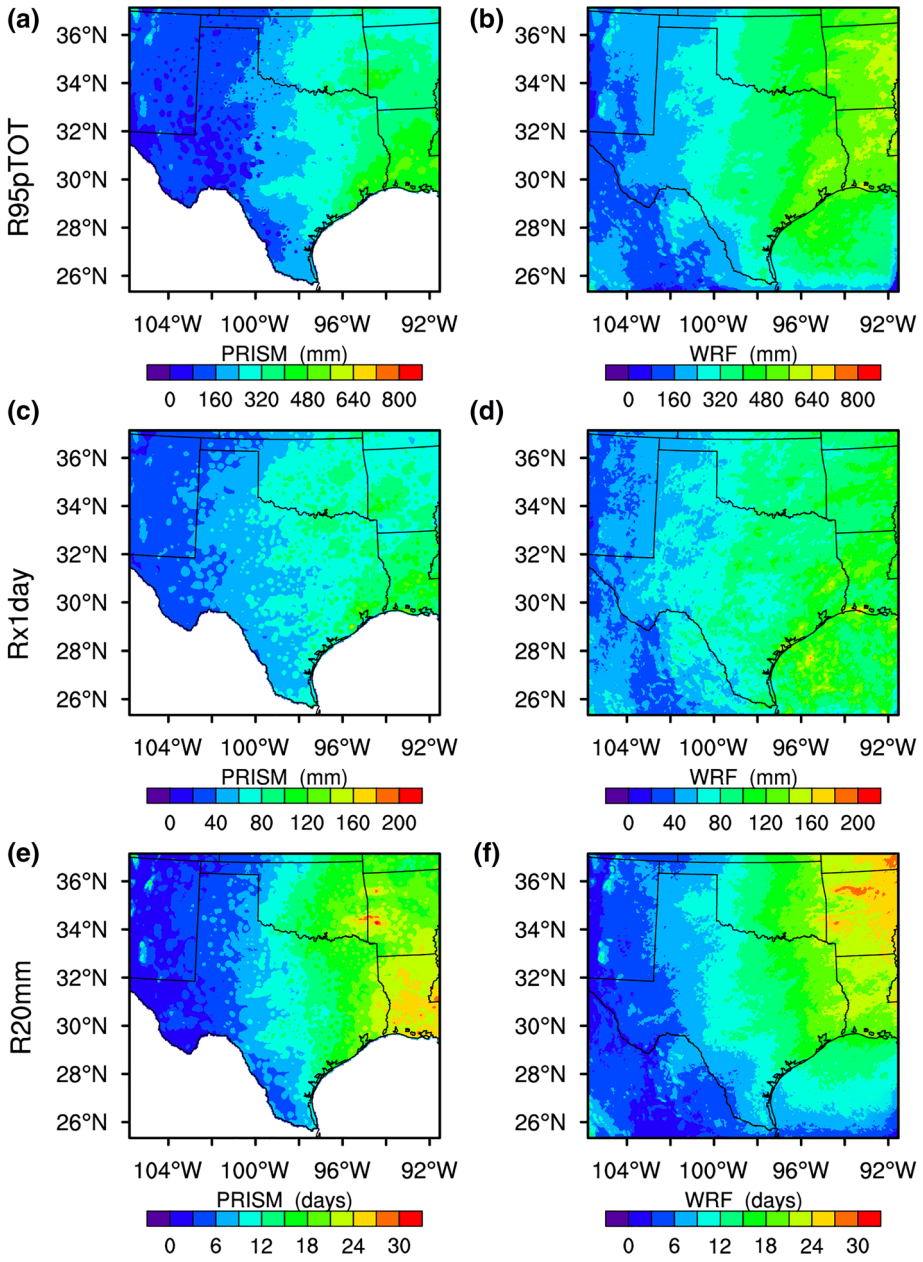

Figure 10. Spatial pattern of 15-year mean precipitation extreme indices (R95pTOT, unit: mm; Rx1day, units: mm; and R20mm, unit: days).

3.4. Projected Changes in Multidimensional Flood Risk

The projected streamflow time series were used to sample flood events using the threshold estimates in Figure S1 together with the corresponding hydrographs. Figure 16 presents the comparison of flood characteristics in past (1981–1995) and future (2085–2099) climates. Guadalupe and Mission river basins experienced 25 and 29 flood events, respectively, for the historical period; 25 and 21 flood events are projected to occur over the two river basins for the future period. The flood peak is projected to decrease whereas both the flood volume and duration are expected to increase for the Guadalupe river basin. In contrast, the flood peak, volume, and duration are expected to increase for the Mission river basin. This implies that Guadalupe and Mission river basins are projected to experience more flood events with longer duration and larger discharge volume even though the frequency of flood events will not increase.

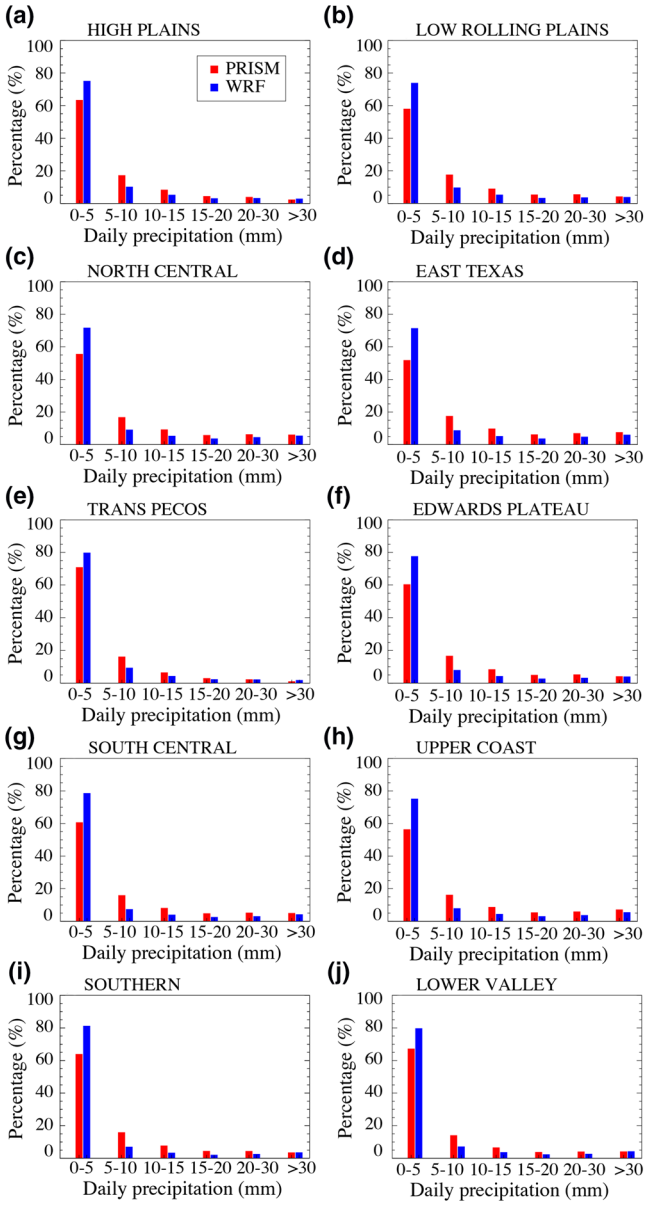

Figure 11. Frequency of daily precipitation from the PRISM observation and the WRF simulation for 10 climate divisions of Texas. WRF, Weather Research and Forecasting.

The multivariate return periods of flood events estimated through the Bayesian vine copula were further used to assess climate change impacts on flood risks. The uncertainties in hydrological simulations, marginal distribution, and the dependence structure between flood variables were integrated into the multidimensional flood risk projections. Figures 17 and 18 present the estimated flood return periods ("AND" and "OR" cases) in past and future climates for Guadalupe and Mission river basins, respectively. Note that the upper bounds of the uncertainty interval depicted in Figures 17 and 18 are truncated for better comparison and visualization. It can be seen that large uncertainties exist in the estimation of return periods, especially for those long return periods. For example, the upper bound of the "AND" case return period for the flood event over the Guadalupe river basin in July 1987 is over 400 years, whereas the corresponding lower bound is ~50 years. The uncertainty is also relatively large for those long return periods since a slight uncertainty for a large joint probability $\Pr(P \geq p^*, V \geq v^*, D \geq d^*)$ can be transformed to a large uncertainty in the return period. In addition, there is no significant change in flood return periods for the Guadalupe river basin between past and future climates, as shown in Figure 17. For example, the mean "OR" case flood return periods between past and future climates are 1.38 and 1.18, respectively (see Figures 17a and 17b). Considering the trivariate "AND" case, the Guadalupe river basin has experienced five 100-year floods during the historical period of 1981–1995 while it is projected to experience three floods of such magnitude for the future period of 2085–2099 (see Figures 17c and 17d). In comparison, Figure 18 shows a remarkable increase in flood return periods for both "AND" and "OR" cases between past and future climates, indicating that the Mission river basin is expected to suffer from higher flood risks under climate change. For example, the maximum "OR" case return period is ~6 years for the future period (Figure 18b) but no flood event has an "OR" case return period of longer than 2 years for the historical period (Figure 18a). More importantly, the Mission river basin is projected to experience approximately seven major floods for the future period of 2085–2099, all of which have the equal or even higher severity as the present-day 100-year floods when considering the "AND" case. This indicates that the Mission river basin will be exposed to 100-year and even severer floods nearly every 2 years, on average, by the end of the 21st century. It should also be noted that such future flood risks are projected under a high emissions pathway (RCP8.5) and would vary by different emission pathways.

Although the extreme precipitation is projected to increase for both Guadalupe and Mission river basins, the dramatic increase of flood risk is only observed for the Mission river basin. Such a difference in flood risk was further investigated by comparing precipitation and soil moisture which are the most important factors affecting floods between past and future climates, as shown in Figure 19. The mean precipitation is expected to decrease for the Guadalupe river basin but to increase for the Mission river basin, both with a small magnitude. However, the right tail of the precipitation distribution shifts obviously rightward only for the Mission river basin (Figure 19b), indicating a relatively larger increase of extreme precipitation over the Mission river basin (also mentioned in Section 3.3). The mean soil moisture is projected to decrease significantly ($P < 0.01$) for the Guadalupe river basin and insignificantly ($P = 0.08$) for the Mission river basin. Therefore, the significantly drying soils can be a potential reason for the projected decrease in flood peaks in spite of the increasing extreme precipitation over the Guadalupe river basin, but this does not necessarily lead to the decrease in flood risks since the flood volume and duration are project-

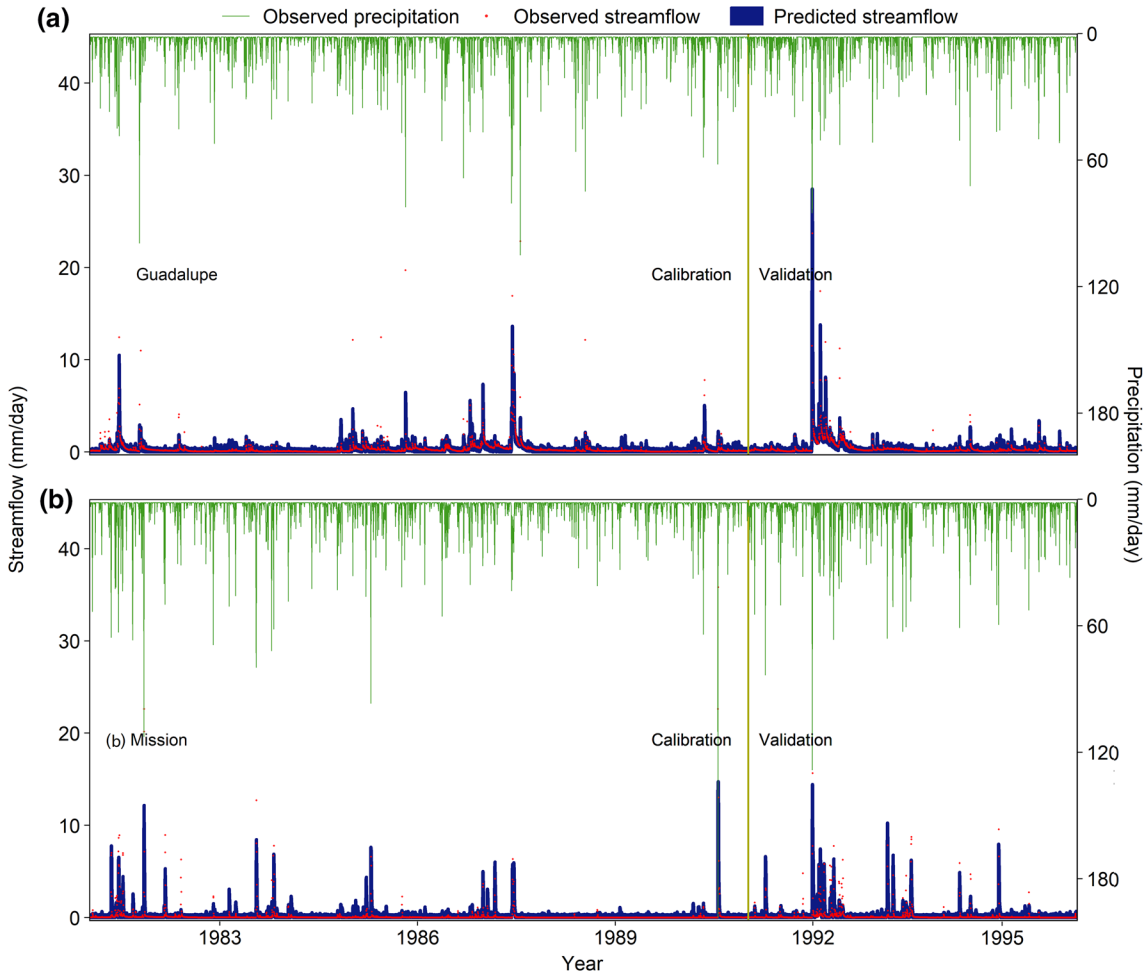

Figure 12. Daily rainfall-runoff simulations for (a) Guadalupe and (b) Mission river basins over South Texas over a period of 15 years (1981–1995). The dark blue area represents the predicted streamflow time series with the 95% uncertainty range. Red dots represent streamflow observations. The green line represents precipitation observations.

ed to increase. The synergies between the relatively strong intensification of extreme precipitation and the little drying of soils lead to the significant increase of flood risk over the Mission river basin.

4. Discussion

4.1. Uncertainty Analysis

The uncertainty in vine copula parameters was addressed using a novel Bayesian vine copula approach, but its influence on the multidimensional flood risk assessment remains elusive. We have compared the 95% uncertainty intervals for the three-dimensional future flood return period with and without considering the uncertainty in vine copula parameters (see Figure S5). Note that the uncertainties in hydrological simulation and marginal distribution were also addressed here. The uncertainty degree for most return periods is not greatly affected by the uncertainty in vine copula parameters. However, the Bayesian vine copula uncovered the substantially amplified uncertainties induced by the vine copula parameters for the high return periods. For example, the projected "AND" case return period for the flood episode in 2093 lies between 11.8 and 9,442 years based on the Bayesian vine copula, whereas the resulting uncertainty interval is [168.6, 2,934] based on the simple vine copula approach. This indicates that the potential risk can be largely underestimated or overestimated by using the simple vine copula approach.

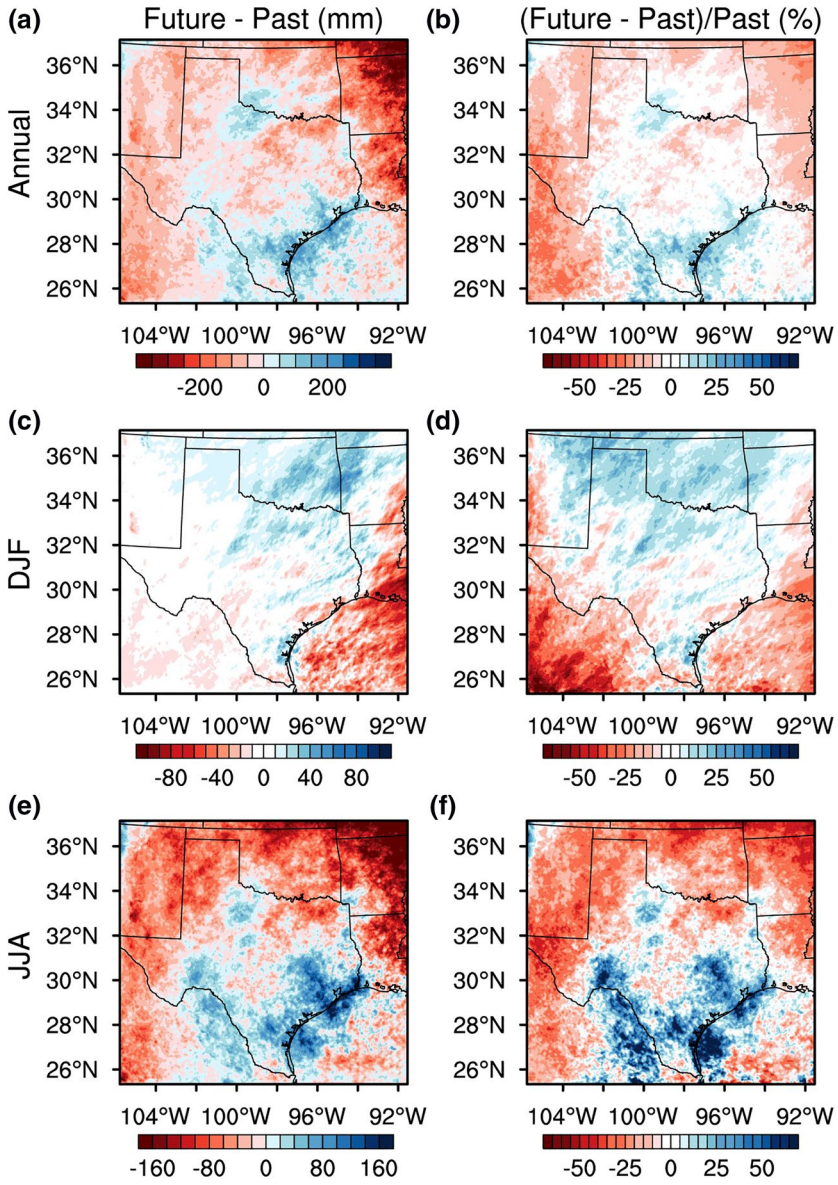

Figure 13. Absolute and relative difference of 15-year annual and seasonal mean precipitation between past and future climates for (a and b) annual, (c and d) DJF, (e and f) June-July-August.

In addition to vine copula parameters, the uncertainties in hydrological simulation and marginal distribution were also addressed. It is thus desired to assess their contribution to the overall uncertainty in the multidimensional flood risk projection. The uncertainty contribution was analyzed based on the three-dimensional "AND" and "OR" case return period of two extreme flood episodes under future climate for each river basin (see Figure S6). Results show that the marginal distribution contributes largely to the overall uncertainty for each case, but the uncertainty contribution of hydrological model parameters is not large as expected especially for the Mission river basin (see Figures S6e–S6h). Although the uncertainty contribution of vine copula parameters is not significant for "OR" cases (Figures S6a, S6b, S6e and S6f), it is significant for "AND" cases and even larger than the marginal distribution (Figures S6c, S6d, S6g, and S6h). Such a large uncertainty contribution of vine copula parameters to the "AND" case can be attributed to three bivariate pair copula CDFs in the return period calculation that is also affected by the uncertainty from vine copula parameters. This further demonstrates that the uncertainty in vine copula parameters cannot be neglected and deserves more attention.

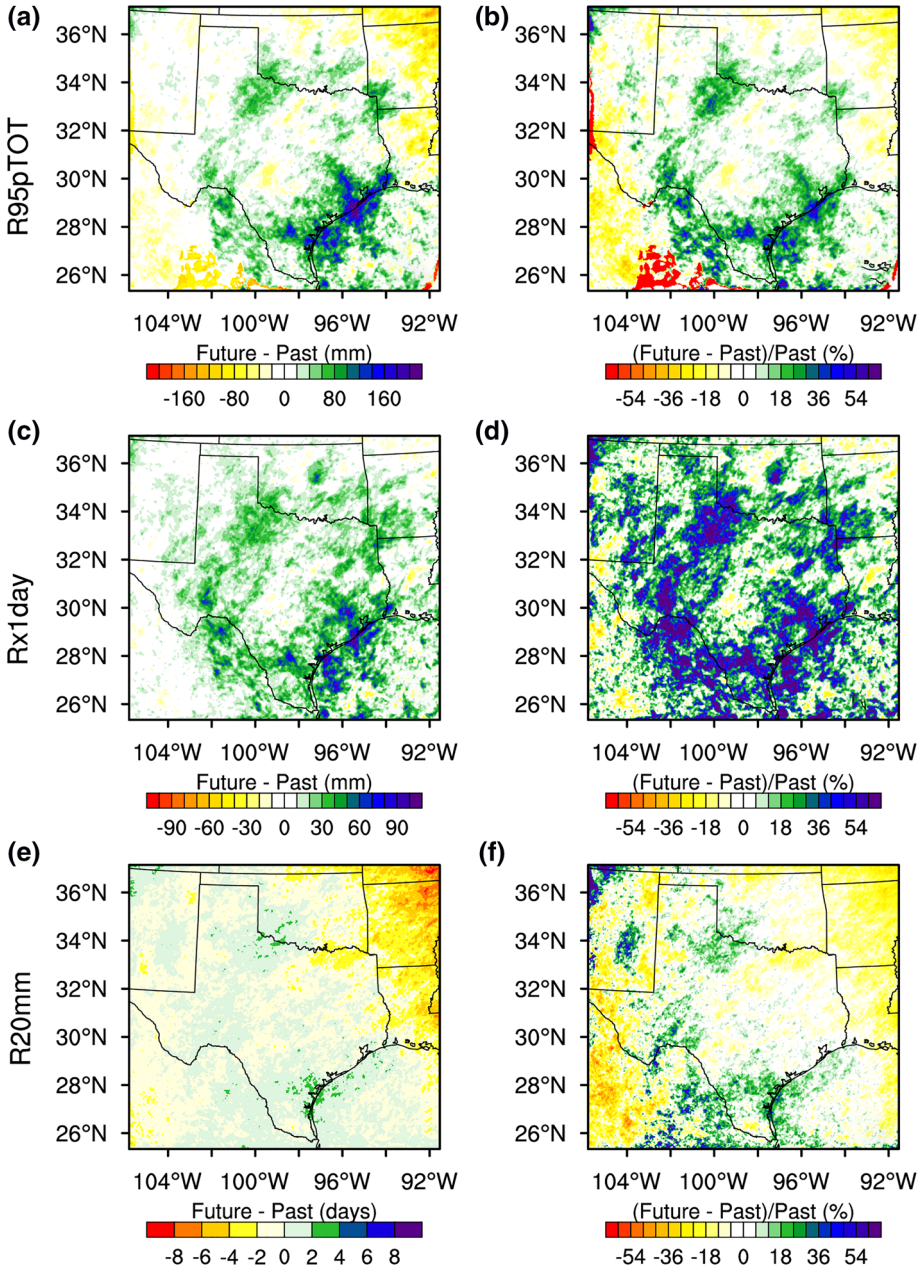

Figure 14. Absolute and relative differences of 15-year mean precipitation extreme (R95pTOT, unit: mm; Rx1day, unit: mm; R20mm, unit: days) between past and future climates. a—b, c—d, and e—f correspond to R95pTOT, Rx1day, and R20mm, respectively.

4.2. Nonstationarity Assessment

As the presence of nonstationary processes in watersheds may lead to biased hydrological simulations, it is desired to assess the transferability of hydrological models under nonstationary conditions. Land use is one of the most important driving forces of hydrological nonstationarity. The transferability of hydrological models was thus evaluated under nonstationary land use patterns through the differential split sample test (DSST). Since the United States experienced persistent urban sprawl in the 20th century (Barrington-Leigh & Millard-Ball, 2015), the first and second half of 1948–2002 (i.e., 1948–1975 and 1976–2002) can be defined as the less and more urbanized period. The Hymod was calibrated for each of the two periods and validated for the other period. Model transferability was evaluated based on the Nash-Sutcliffe Efficiency (NSE)

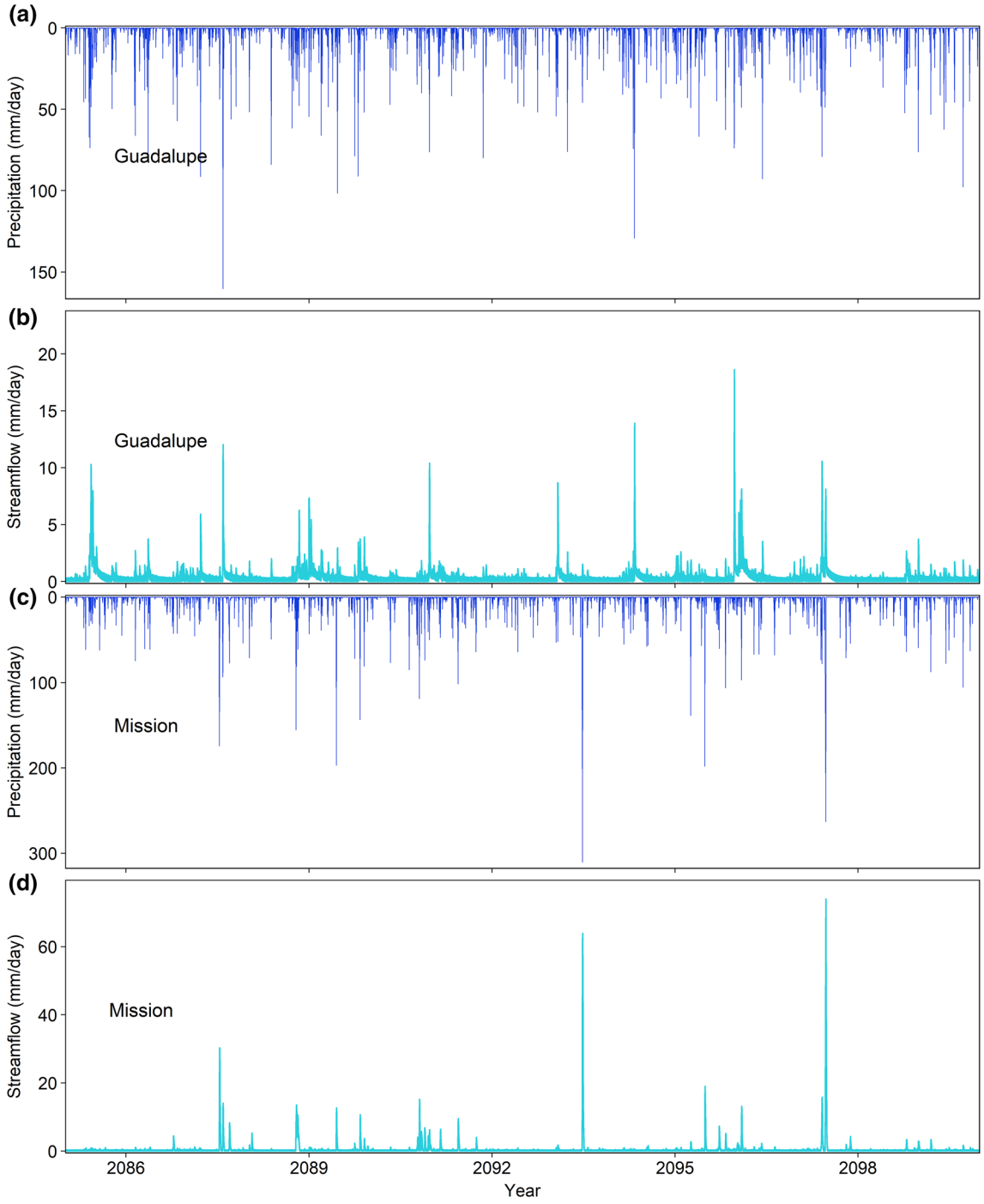

Figure 15. Daily rainfall-runoff projections for Guadalupe (a and b) and Mission (c and d) river basins over South Texas by the end of the 21st century. The light blue area and the dark blue line represent the projected streamflow and precipitation, respectively.

metric, the cumulated volume error (VE), and the fraction of measured data with the 95% uncertainty interval (hereafter referred to as *p*-factor). Daily streamflow simulations calibrated during 1948–1975 (1976–2002) and validated during 1976–2002 (1948–1975) for Guadalupe and Mission river basins are shown in Figures S7 and S8, respectively. Results show that there is no obvious difference between calibration and validation results for each period at each river basin (e.g., Figures S7b and S8c). In addition, there is no consistent change in model performance between calibration and validation periods based on the three

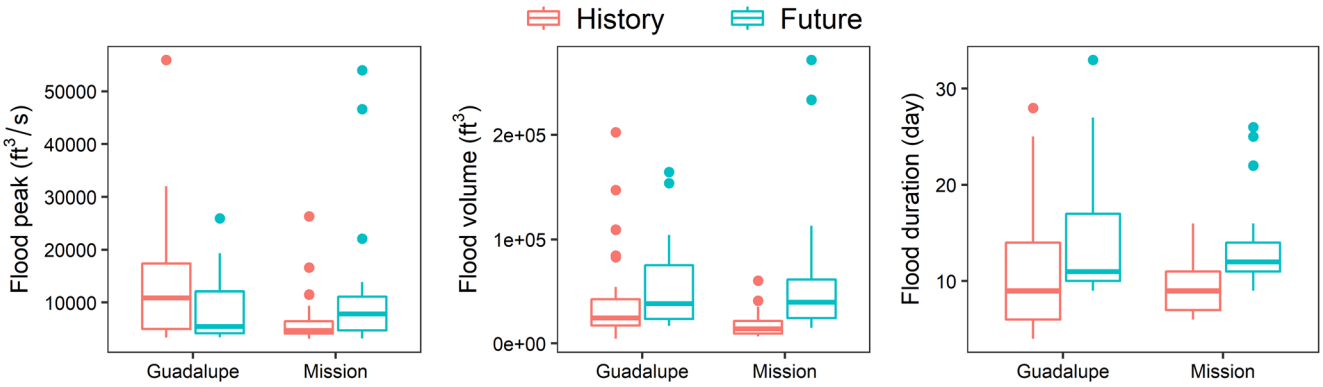

Figure 16. Comparison of flood characteristics in past and future climates.

different criteria. This indicates that the difference in land use patterns between calibration and validation periods has no obvious negative impact on model performance for Guadalupe and Mission river basins. Model transferability is thus acceptable in the study area, and can lead to reasonable hydrological projections. In addition, the issue of nonstationary depends on a variety of factors, including the magnitude of future climate change and land use change, the length and variability of the historical record, the hydrological model deficiency, and others (Dakhlaoui et al., 2017; Gharari et al., 2013; Milly et al., 2008, 2015; Serinaldi & Kilsby, 2015; Westra et al., 2014). To further improve the credibility of hydrological projections, it is desired to perform a comprehensive evaluation of hydrological model transferability under different climate conditions and different land use patterns in our future studies.

The proposed Bayesian vine copula assumes that the multivariate flood characteristics are stationary, which can be violated due to the changes in hydrometeorological processes. To assess the assumption of stationarity in multivariate flood risk projections, the univariate and multivariate Mann–Kendall trend tests were used to capture all existing trend components in the trivariate vine copula as the signs of nonstationarity (see Table S5). It can be seen that no component presents a significant trend at the significance level of 0.05 except for the flood duration over Mission river basin. This indicates that nearly all components are stationary in the multivariate flood assessments and thus the stationarity assumption is acceptable in this study. In addition, the presence of nonstationarity has received increasing attention in multivariate hydrological analysis. It is thus desired to extend the proposed stationary vine copula framework into nonstationary one for dynamic flood risk assessment in future studies.

5. Summary and Conclusions

In this study, we developed probabilistic projections of future changes in multidimensional flood risks at a convection-permitting scale. Future climate change information was projected using the convection-permitting WRF model with horizontal grid spacing of 4 km, which was then used to drive the hydrological model for producing probabilistic streamflow projections for two major river basins over South Texas. The Peaks over Threshold (POT) method was used to carry out flood event sampling, and a Bayesian vine copula was proposed to provide a robust assessment of the multidimensional dependence of flood variables including flood peak, volume, and duration. The underlying uncertainty in vine copula parameters was explicitly addressed using the MCMC simulation. In addition, we examined the relative contribution of uncertainties in hydrological simulations, marginal distributions, and vine copula parameters to the overall uncertainty of multidimensional flood risk assessment.

The proposed Bayesian vine copula improves upon flood risk assessments not only by taking into account the multidimensional flood characteristics and their interactions but also by addressing the underlying uncertainties in pair-copula parameters and the marginal fitting. Our findings indicate that the frequentist vine copula approach can generate plausible simulations but neglect the other equally acceptable simulations, which can underestimate the return periods of flood events and thus pose a considerable risk to the

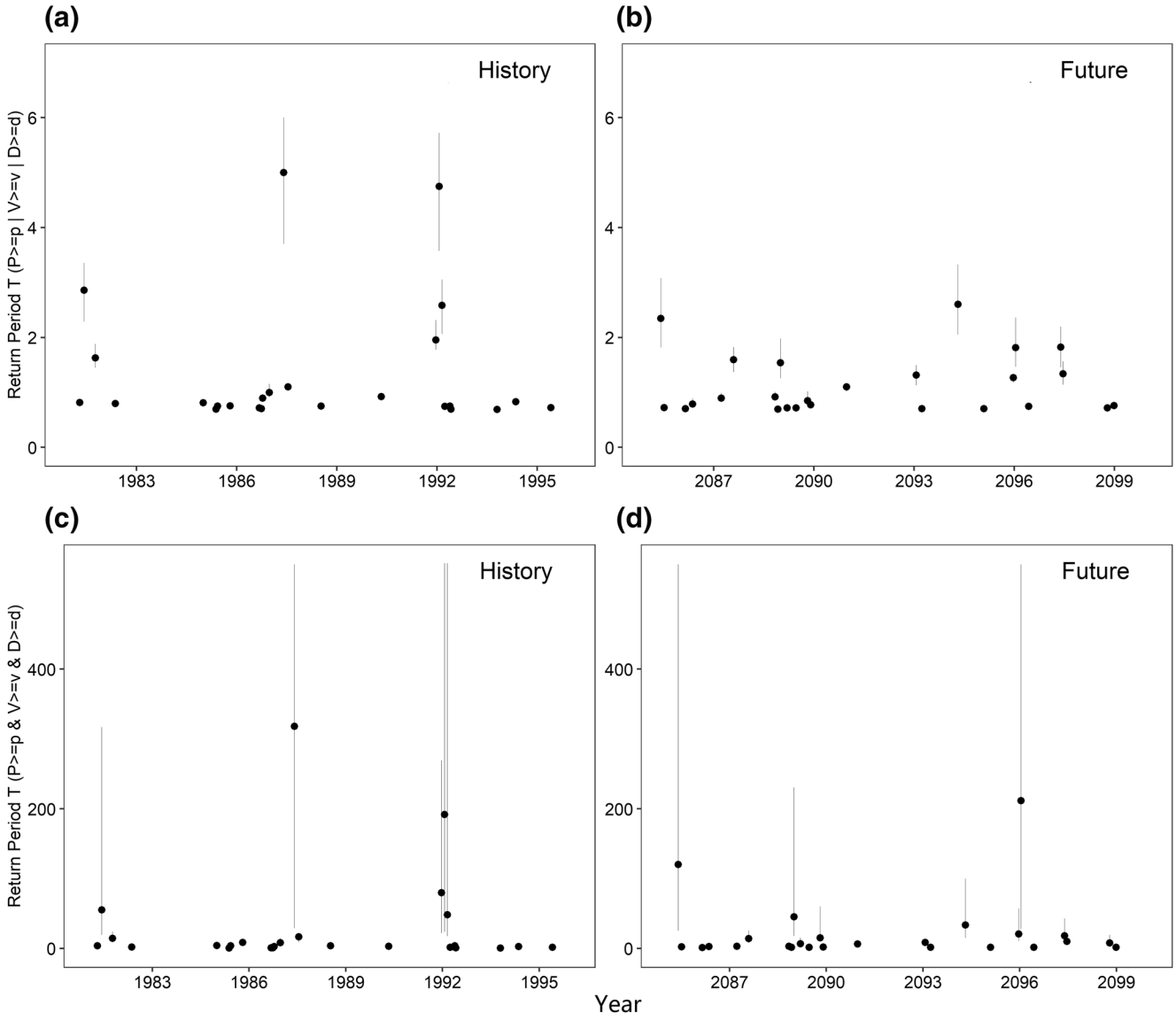

Figure 17. Comparison of the three-dimensional flood return period including "OR" (a and b) and "AND" (c and d) cases in past and future climates for Guadalupe river basin. The gray lines represent the 95% uncertainty range owing to the underlying uncertainties in hydrological simulations, marginal distributions, and vine copula parameters. The black points represent the median return periods.

hydrologic design. The uncertainty in pair-copula parameters cannot be ignored even though it is relatively small compared to the uncertainty in the marginal fitting. In addition, the convection-permitting climate simulation significantly outperforms the CFSR data set in well reproducing the observed long-term mean and short-term extreme precipitation owing to its ability to explicitly resolve convection processes and to characterize the kilometer-scale spatial heterogeneity. Since flood events typically originate from extreme precipitation, the accurate simulation of precipitation is crucial to enhancing the reliability of flood risk assessment and projection.

The high-resolution precipitation projection indicates that the frequency and intensity of extreme precipitation are expected to increase, but the total number of rainy days will decrease in a changing climate. In addition, the flood volume and duration are expected to increase while the flood peak will not necessarily increase. Specifically, there is no significant increase in the multidimensional return periods of flood events over the Guadalupe river basin. In contrast, the Mission river basin is projected to face a severe increase in flood risk with exposed to 100-year and even severer floods nearly every 2 years, on average. Such a large

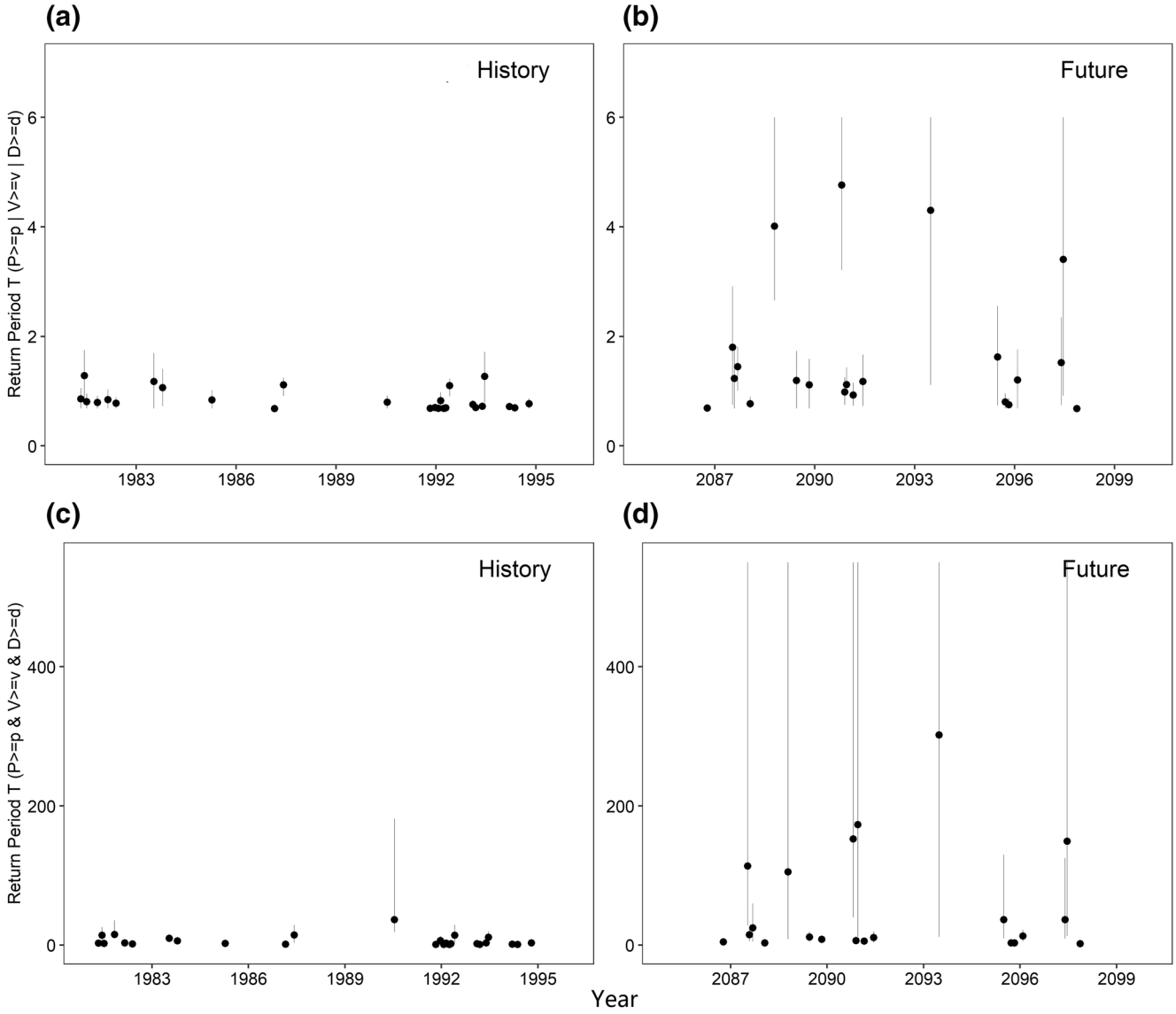

Figure 18. Comparison of the three-dimensional flood return period including "OR" (a and b) and "AND" (c and d) cases in past and future climates for Mission river basin. The gray lines represent the 95% uncertainty range owing to the underlying uncertainties in hydrological simulations, marginal distributions, and vine copula parameters. The black points represent the median return periods.

difference in the projected change of flood risk for Guadalupe and Mission river basins can be attributed to the different climate responses of extreme precipitation and soil moisture.

It should be noted that the uncertainty of the vine structure in the vine copula simulation is not explicitly addressed in this study although the optimal vine structure is identified. Efforts are underway for conducting a thorough analysis of different sources of uncertainty in the vine copula simulation, including the vine structure, the pair-copula parameter, the marginal fitting, and the observation, in order to further improve the reliability of flood risk assessment and projection. In addition, the convection-permitting climate projections were carried out under RCP8.5 which was the "business-as-usual" climate scenario. The uncertainty in emission scenarios was not addressed, which was considered as a limitation of this study due to the extremely high computational cost of convection-permitting climate simulations. Future studies would thus be undertaken to account for multiple emission scenarios to improve the robustness of flood risk projections when the high-performance computing resources become available.

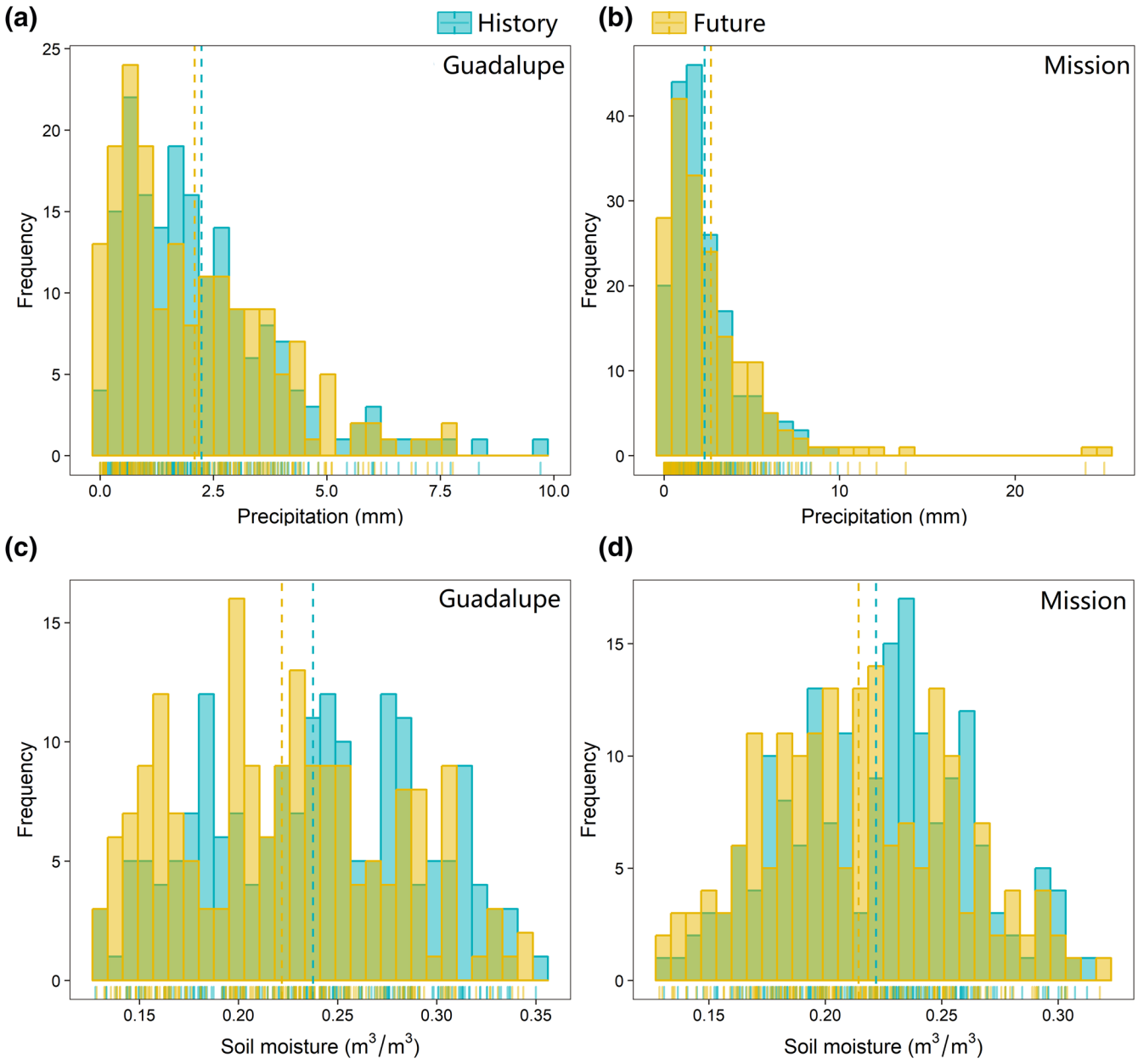

Figure 19. Frequency of monthly precipitation and soil moisture for Guadalupe (a and c) and Mission (b and d) river basins between past and future climates.

Data Availability Statement

The PRISM data set was provided by the NOAA/OAR/ESRL PSD, Boulder, Colorado, USA and can be downloaded at http://prism.oregonstate.edu/recent/. The CFSR data set was developed by NOAA's National Centers for Environmental Prediction (NCEP) and can be downloaded at https://rda.ucar.edu/datasets/ds093.1/. The daily hydrological data for Guadalupe and Mission river basins were collected from the U.S. MOPEX data set (https://www.nws.noaa.gov/ohd/mopex/mo_datasets.htm) and the United States Geological Survey (USGS) river flow gauging stations (https://waterdata.usgs.gov/nwis/uv/?referred_module=sw). The WRF model outputs over the streamflow gauge stations and other related data used in this study are available in Zhang (2020), https://doi.org/10.17632/csdctns7wj.2. The source code of the proposed methodology is available from the GitHub (https://github.com/Boorn123/PolyU-Hydroclimate/blob/master/code/BayesianVineCopulaFlood.R).

Acknowledgments
This research was supported by the National Natural Science Foundation of China (Grant No. 51809223) and the Hong Kong Research Grants Council Early Career Scheme (Grant PP5Z). We acknowledge the World Climate Research Programme's Working Group on Coupled Modeling, which is responsible for CMIP5, and we thank the climate modeling groups for producing and making their model outputs available at https://esgf-node.llnl.gov/projects/cmip5/. We would like to express our sincere gratitude to the associate editor and five anonymous reviewers for their constructive comments and suggestions.

References

Aas, K., Czado, C., Frigessi, A., & Bakken, H. (2009). Pair-copula constructions of multiple dependence. *Insurance: Mathematics and Economics*, *44*(2), 182–198. https://doi.org/10.1016/j.insmatheco.2007.02.001

Alfieri, L., Bisselink, B., Dottori, F., Naumann, G., de Roo, A., Salamon, P., et al. (2017). Global projections of river flood risk in a warmer world. *Earth's Future*, *5*, 171–182. https://doi.org/10.1002/2016EF000485

Alfieri, L., Burek, P., Feyen, L., & Forzieri, G. (2015). Global warming increases the frequency of river floods in Europe. *Hydrology and Earth System Sciences*, *19*(5), 2247–2260. https://doi.org/10.5194/hess-19-2247-2015

Allen, R. G., Pereira, L. S., Raes, D., & Smith, M. (1998). Crop evapotranspiration—Guidelines for computing crop water requirements—FAO irrigation and drainage paper 56. *FAO, Rome*, *300*(9), D05109.

Balistrocchi, M., Orlandini, S., Ranzi, R., & Bacchi, B. (2017). Copula-based modeling of flood control reservoirs. *Water Resources Research*, *53*, 9883–9900. https://doi.org/10.1002/2017WR021345

Barrington-Leigh, C., & Millard-Ball, A. (2015). A century of sprawl in the United States. *Proceedings of the National Academy of Sciences of the United States of America*, *112*(27), 8244–8249. https://doi.org/10.1073/pnas.1504033112

Bedford, T., & Cooke, R. M. (2002). Vines—A new graphical model for dependent random variables. *Annals of Statistics*, *30*(4), 1031–1068. https://doi.org/10.1214/aos/1031689016

Bevacqua, E., Maraun, D., Hobæk Haff, I., Widmann, M., & Vrac, M. (2017). Multivariate statistical modeling of compound events via pair-copula constructions: Analysis of floods in Ravenna (Italy). *Hydrology and Earth System Sciences*, *21*(6), 2701–2723. https://doi.org/10.5194/hess-21-2701-2017

Blöschl, G., Hall, J., Viglione, A., Perdigão, R. A. P., Parajka, J., Merz, B., et al. (2019). Changing climate both increases and decreases European river floods. *Nature*, *573*(7772), 108–111. https://doi.org/10.1038/s41586-019-1495-6

Brisson, E., Van Weverberg, K., Demuzere, M., Devis, A., Saeed, S., Stengel, M., & van Lipzig, N. P. M. (2016). How well can a convection-permitting climate model reproduce decadal statistics of precipitation, temperature and cloud characteristics? *Climate Dynamics*, *47*(9–10), 3043–3061. https://doi.org/10.1007/s00382-016-3012-z

Brunner, M. I., Hingray, B., Zappa, M., & Favre, A. C. (2019). Future trends in the interdependence between flood peaks and volumes: Hydro-climatological drivers and uncertainty. *Water Resources Research*, *55*, 4745–4759. https://doi.org/10.1029/2019WR024701

Carvalho, K. S., & Wang, S. (2019). Characterizing the Indian Ocean sea level changes and potential coastal flooding impacts under global warming. *Journal of Hydrology*, *569*, 373–386. https://doi.org/10.1016/j.jhydrol.2018.11.072

Chen, H., Wang, S., & Wang, Y. (2020a). Exploring abrupt alternations between wet and dry conditions on the basis of historical observations and convection-permitting climate model simulations. *Journal of Geophysical Research: Atmospheres*, *125*, e2019JD031982. https://doi.org/10.1029/2019JD031982

Chen, H., Wang, S., Zhu, J., & Zhang, B. (2020b). Projected changes in abrupt shifts between dry and wet extremes over China through an ensemble of regional climate model simulations. *Journal of Geophysical Research: Atmospheres*, *125*, e2020JD033894. https://doi.org/10.1029/2020JD033894

Dakhlaoui, H., Ruelland, D., Tramblay, Y., & Bargaoui, Z. (2017). Evaluating the robustness of conceptual rainfall-runoff models under climate variability in northern Tunisia. *Journal of Hydrology*, *550*, 201–217. https://doi.org/10.1016/j.jhydrol.2017.04.032

Daly, C., Neilson, R. P., & Phillips, D. L. (1994). A statistical-topographic model for mapping climatological precipitation over mountainous terrain. *Journal of Applied Meteorology*, *33*(2), 140–158. https://doi.org/10.1175/1520-0450(1994)033<0140:ASTMFM>2.0.CO;2

Daneshkhah, A., Remesan, R., Chatrabgoun, O., & Holman, I. P. (2016). Probabilistic modeling of flood characterizations with parametric and minimum information pair-copula model. *Journal of Hydrology*, *540*, 469–487. https://doi.org/10.1016/j.jhydrol.2016.06.044

Dechant, C. M., & Moradkhani, H. (2015). On the assessment of reliability in probabilistic hydrometeorological event forecasting. *Water Resources Research*, *51*, 3867–3883. https://doi.org/10.1002/2014WR016617

Duan, Q., Schaake, J., Andréassian, V., Franks, S., Goteti, G., Gupta, H. V., et al. (2006). Model Parameter Estimation Experiment (MOPEX): An overview of science strategy and major results from the second and third workshops. *Journal of Hydrology*, *320*(1–2), 3–17. https://doi.org/10.1016/j.jhydrol.2005.07.031

Farmer, W. H., & Vogel, R. M. (2016). On the deterministic and stochastic use of hydrologic models. *Water Resources Research*, *52*, 5619–5633. https://doi.org/10.1002/2016WR019129

Favre, A. C., Adlouni, S. E., Perreault, L., Thiémonge, N., & Bobée, B. (2004). Multivariate hydrological frequency analysis using copulas. *Water Resources Research*, *40*, W01101. https://doi.org/10.1029/2003WR002456

Fosser, G., Khodayar, S., & Berg, P. (2014). Benefit of convection permitting climate model simulations in the representation of convective precipitation. *Climate Dynamics*, *44*(1–2), 45–60. https://doi.org/10.1007/s00382-014-2242-1

Gelman, A., & Rubin, D. B. (1992). Inference from iterative simulation using multiple sequences. *Statistical Science*, *7*(4), 457–472. https://doi.org/10.1214/ss/1177011136

Genest, C., Favre, A. C., Béliveau, J., & Jacques, C. (2007). Metaelliptical copulas and their use in frequency analysis of multivariate hydrological data. *Water Resources Research*, *43*, W09401. https://doi.org/10.1029/2006WR005275

Gharari, S., Hrachowitz, M., Fenicia, F., & Savenije, H. H. G. (2013). An approach to identify time consistent model parameters: Sub-period calibration. *Hydrology and Earth System Sciences*, *17*(1), 149–161. https://doi.org/10.5194/hess-17-149-2013

Giorgi, F. (2019). Thirty years of regional climate modeling: Where are we and where are we going next? *Journal of Geophysical Research: Atmospheres*, *124*, 5696–5723. https://doi.org/10.1029/2018JD030094

Gruber, L., & Czado, C. (2015). Sequential Bayesian model selection of regular vine copulas. *Bayesian Analysis*, *10*(4), 937–963.

Gruber, L., & Czado, C. (2018). Bayesian model selection of regular vine copulas. *Bayesian Analysis*, *13*(4), 1107–1131. https://doi.org/10.1214/17-BA1089

Guadalupe-Blaco River Authority (GBRA) (n.d.) *Staying safe.. A guide for flooding in the Guadalupe river basin*. Seguin, TX. Retrieved from http://www.gbra.org/documents/flood/stayingsafe.pdf

Hara, M., Yoshikane, T., Kawase, H., & Kimura, F. (2008). Estimation of the impact of global warming on snow depth in Japan by the pseudo-global-warming method. *Hydrological Research Letters*, *2*, 61–64. https://doi.org/10.3178/hrl.2.61

Herman, J. D., Reed, P. M., & Wagener, T. (2013). Time-varying sensitivity analysis clarifies the effects of watershed model formulation on model behavior. *Water Resources Research*, *49*, 1400–1414. https://doi.org/10.1002/wrcr.20124

Hirabayashi, Y., Mahendran, R., Koirala, S., Konoshima, L., Yamazaki, D., Watanabe, S., et al. (2013). Global flood risk under climate change. *Nature Climate Change*, *3*(9), 816–821. https://doi.org/10.1038/nclimate1911

Hobæk Haff, I., & Segers, J. (2015). Nonparametric estimation of pair-copula constructions with the empirical pair-copula. *Computational Statistics & Data Analysis*, *84*, 1–13. https://doi.org/10.1016/j.csda.2014.10.020

Huang, K., Ye, L., Chen, L., Wang, Q., Dai, L., Zhou, J., et al. (2018). Risk analysis of flood control reservoir operation considering multiple uncertainties. *Journal of Hydrology*, *565*, 672–684. https://doi.org/10.1016/j.jhydrol.2018.08.040

Jeong, D. I., Sushama, L., Khaliq, M. N., & Roy, R. (2014). A copula-based multivariate analysis of Canadian RCM projected changes to flood characteristics for northeastern Canada. *Climate Dynamics*, *42*(7–8), 2045–2066. https://doi.org/10.1007/s00382-013-1851-4

Jiang, C., Xiong, L., Yan, L., Dong, J., & Xu, C. Y. (2019). Multivariate hydrologic design methods under nonstationary conditions and application to engineering practice. *Hydrology and Earth System Sciences*, *23*(3), 1683–1704. https://doi.org/10.5194/hess-23-1683-2019

Joe, H. (1996). Families of m-variate distributions with given margins and m(m-1)/2 bivariate dependence parameters. *Lecture Notes-Monograph Series*, *28*, 120–141.

Jongman, B., Winsemius, H. C., Aerts, J. C. J. H., Coughlan De Perez, E., Van Aalst, M. K., Kron, W., & Ward, P. J. (2015). Declining vulnerability to river floods and the global benefits of adaptation. *Proceedings of the National Academy of Sciences of the United States of America*, *112*(18), E2271–E2280. https://doi.org/10.1073/pnas.414439112

Lauer, A., Zhang, C., Elison-Timm, O., Wang, Y., & Hamilton, K. (2013). Downscaling of climate change in the Hawaii region using CMIP5 results: On the choice of the forcing fields. *Journal of Climate*, *26*(24), 10006–10030. https://doi.org/10.1175/JCLI-D-13-00126.1

Lin, P., Hopper, L. J., Yang, Z. L., Lenz, M., & Zeitler, J. W. (2018a). Insights into hydrometeorological factors constraining flood prediction skill during the May and October 2015 Texas Hill Country flood events. *Journal of Hydrometeorology*, *19*(8), 1339–1361. https://doi.org/10.1175/JHM-D-18-0038.1

Lin, P., Rajib, M. A., Yang, Z. L., Somos-Valenzuela, M., Merwade, V., Maidment, D. R., et al. (2018b). Spatiotemporal evaluation of simulated evapotranspiration and streamflow over Texas using the WRF-Hydro-RAPID modeling framework. *Journal of the American Water Resources Association*, *54*(1), 40–54. https://doi.org/10.1111/1752-1688.12585

Liu, C., Ikeda, K., Rasmussen, R., Barlage, M., Newman, A. J., Prein, A. F., et al. (2017). Continental-scale convection-permitting modeling of the current and future climate of North America. *Climate Dynamics*, *49*(1–2), 71–95.

Liu, Z., Cheng, L., Hao, Z., Li, J., Thorstensen, A., & Gao, H. (2018). A framework for exploring joint effects of conditional factors on compound floods. *Water Resources Research*, *54*, 2681–2696. https://doi.org/10.1002/2017WR021662

Liu, Z., Zhou, P., Chen, X., & Guan, Y. (2015). A multivariate conditional model for streamflow prediction and spatial precipitation refinement. *Journal of Geophysical Research: Atmospheres*, *120*, 10116–10129. https://doi.org/10.1002/2015JD023787

Mallakpour, I., AghaKouchak, A., & Sadegh, M. (2019). Climate-induced changes in the risk of hydrological failure of major dams in California. *Geophysical Research Letters*, *46*, 2130–2139. https://doi.org/10.1029/2018GL081888

Marsooli, R., Lin, N., Emanuel, K., & Feng, K. (2019). Climate change exacerbates hurricane flood hazards along US Atlantic and Gulf Coasts in spatially varying patterns. *Nature Communications*, *10*(1), 3785. https://doi.org/10.1038/s41467-019-11755-z

McKay, M. D., Beckman, R. J., & Conover, W. J. (1979). Comparison of three methods for selecting values of input variables in the analysis of output from a computer code. *Technometrics*, *21*(2), 239–245.

Milly, P. C. D., Betancourt, J., Falkenmark, M., Hirsch, R. M., Kundzewicz, Z. W., Lettenmaier, D. P., et al. (2015). On Critiques of "stationarity is dead: Whither water management?". *Water Resources Research*, *51*, 7785–7789. https://doi.org/10.1002/2015WR017408

Milly, P. C. D., Betancourt, J., Falkenmark, M., Hirsch, R. M., Kundzewicz, Z. W., Lettenmaier, D. P., & Stouffer, R. J. (2008). Climate change: Stationarity is dead: Whither water management? *Science*. *319*(5863), 573–574. https://doi.org/10.1126/science.1151915

Min, A., & Czado, C. (2010). Bayesian inference for multivariate copulas using pair-copula constructions. *Journal of Financial Econometrics*, *8*(4), 511–546. https://doi.org/10.1093/jjfinec/nbp031

Moftakhari, H. R., Salvadori, G., AghaKouchak, A., Sanders, B. F., & Matthew, R. A. (2017). Compounding effects of sea level rise and fluvial flooding. *Proceedings of the National Academy of Sciences of the United States of America*, *114*(37), 9785–9790. https://doi.org/10.1073/pnas.1620325114

Moss, R. H., Edmonds, J. A., Hibbard, K. A., Manning, M. R., Rose, S. K., Van Vuuren, D. P., et al. (2010). The next generation of scenarios for climate change research and assessment. *Nature*, *463*, 747–756. https://doi.org/10.1038/nature08823

Mulligan, M., van Soesbergen, A., & Sáenz, L. (2020). GOODD, a global dataset of more than 38,000 georeferenced dams. *Scientific Data*, *7*, 31. https://doi.org/10.1038/s41597-020-0362-5

Nagler, T., Schepsmeier, U., Stoeber, J., Brechmann, E. C., Graeler, B., & Erhardt, T. (2019). *VineCopula: Statistical inference of vine copulas. R package version 2.3.0.* Retrieved from https://cran.r-project.org/package=VineCopula

Prein, A. F., Gobiet, A., Suklitsch, M., Truhetz, H., Awan, N. K., Keuler, K., & Georgievski, G. (2013). Added value of convection permitting seasonal simulations. *Climate Dynamics*, *41*(9–10), 2655–2677. https://doi.org/10.1007/s00382-013-1744-6

Prein, A. F., Rasmussen, R. M., Ikeda, K., Liu, C., Clark, M. P., & Holland, G. J. (2017). The future intensification of hourly precipitation extremes. *Nature Climate Change*, *7*(1), 48–52. https://doi.org/10.1038/nclimate3168

Qing, Y., Wang, S., Zhang, B., & Wang, Y. (2020). Ultra-high resolution regional climate projections for assessing changes in hydrological extremes and underlying uncertainties. *Climate Dynamics*, *55*(7–8), 2031–2051. https://doi.org/10.1007/s00382-020-05372-6

Quinn, N., Bates, P. D., Neal, J., Smith, A., Wing, O., Sampson, C., et al. (2019). The spatial dependence of flood hazard and risk in the United States. *Water Resources Research*, *55*, 1890–1911. https://doi.org/10.1029/2018WR024205

Raff, D. A., Pruitt, T., & Brekke, L. D. (2009). A framework for assessing flood frequency based on climate projection information. *Hydrology and Earth System Sciences*, *13*(11), 2119–2136. https://doi.org/10.5194/hess-13-2119-2009

Ramos, M. H., Van Andel, S. J., & Pappenberger, F. (2013). Do probabilistic forecasts lead to better decisions? *Hydrology and Earth System Sciences*, *17*(6), 2219–2232. https://doi.org/10.5194/hess-17-2219-2013

Roy, T., Serrat-Capdevila, A., Gupta, H., & Valdes, J. (2017). A platform for probabilistic multimodel and multiproduct streamflow forecasting. *Water Resources Research*, *53*, 376–399. https://doi.org/10.1002/2016WR019752

Sadegh, M., Ragno, E., & AghaKouchak, A. (2017). Multivariate Copula Analysis Toolbox (MvCAT): Describing dependence and underlying uncertainty using a Bayesian framework. *Water Resources Research*, *53*, 5166–5183. https://doi.org/10.1002/2016WR020242

Salas, F. R., Somos-Valenzuela, M. A., Dugger, A., Maidment, D. R., Gochis, D. J., David, C. H., et al. (2018). Toward real-time continental scale streamflow simulation in continuous and discrete space. *Journal of the American Water Resources Association*, *54*(1), 7–27. https://doi.org/10.1111/1752-1688.12586

Salvadori, G., & De Michele, C. (2004). Frequency analysis via copulas: Theoretical aspects and applications to hydrological events. *Water Resources Research*, *40*, W12511. https://doi.org/10.1029/2004WR003133

Salvadori, G., Durante, F., De Michele, C., Bernardi, M., & Petrella, L. (2016). A multivariate copula-based framework for dealing with hazard scenarios and failure probabilities. *Water Resources Research*, *52*, 3701–3721. https://doi.org/10.1002/2015WR017225

Santhosh, D., & Srinivas, V. V. (2013). Bivariate frequency analysis of floods using a diffusion based kernel density estimator. *Water Resources Research*, *49*, 8328–8343. https://doi.org/10.1002/2011WR010777

Serinaldi, F., & Kilsby, C. G. (2013). The intrinsic dependence structure of peak, volume, duration, and average intensity of hyetographs and hydrographs. *Water Resources Research*, *49*, 3423–3442. https://doi.org/10.1002/wrcr.20221

Serinaldi, F., & Kilsby, C. G. (2015). Stationarity is undead: Uncertainty dominates the distribution of extremes. *Advances in Water Resources*, *77*, 17–36. https://doi.org/10.1016/j.advwatres.2014.12.013

Sharma, A., Wasko, C., & Lettenmaier, D. P. (2018). If precipitation extremes are increasing, why aren't floods? *Water Resources Research*, *54*, 8545–8551. https://doi.org/10.1029/2018WR023749

Shkolnik, I., Pavlova, T., Efimov, S., & Zhuravlev, S. (2018). Future changes in peak river flows across northern Eurasia as inferred from an ensemble of regional climate projections under the IPCC RCP8.5 scenario. *Climate Dynamics*, *50*(1–2), 215–230. https://doi.org/10.1007/s00382-017-3600-6

Sklar, A. (1959). *Fonctions de r{é}partition {à} {n} dimensions et leurs marges (Distribution functions of {n} dimensions and their marginals)*. Publications de l'Institut Statistique de l'Universit{é} de Paris.

Smith, A. B. (2020). *U.S. Billion-dollar weather and climate disasters, 1980-present (NCEI Accession 0209268)*. NOAA National Centers for Environmental Information. Dataset. https://doi.org/10.25921/stkw-7w73

Solari, S., Egüen, M., Polo, M. J., & Losada, M. A. (2017). Peaks Over Threshold (POT): A methodology for automatic threshold estimation using goodness of fit p-value. *Water Resources Research*, *53*, 2833–2849. https://doi.org/10.1002/2016WR019426

Texas Floodplain Management Association (TFMA). (2015). *Quick guide: Floodplain management in Texas*. Retrieved from https://www.twdb.texas.gov/flood/resources/doc/Texas_Quick_Guide.pdf

Vrugt, J. A. (2016). Markov chain Monte Carlo simulation using the DREAM software package: Theory, concepts, and MATLAB implementation. *Environmental Modelling & Software*, *75*, 273–316. https://doi.org/10.1016/j.envsoft.2015.08.013

Vrugt, J. A., ter Braak, C. J. F., Clark, M. P., Hyman, J. M., & Robinson, B. A. (2008). Treatment of input uncertainty in hydrologic modeling: Doing hydrology backward with Markov chain Monte Carlo simulation. *Water Resources Research*, *44*, W00B09. https://doi.org/10.1029/2007WR006720

Wagner, S., Berg, P., Schädler, G., & Kunstmann, H. (2013). High resolution regional climate model simulations for Germany: Part II-projected climate changes. *Climate Dynamics*, *40*(1–2), 415–427. https://doi.org/10.1007/s00382-012-1510-1

Wang, S., Ancell, B. C., Huang, G. H., & Baetz, B. W. (2018). Improving robustness of hydrologic ensemble predictions through probabilistic pre- and post-processing in sequential data assimilation. *Water Resources Research*, *54*, 2129–2151. https://doi.org/10.1002/2018WR022546

Wang, S., & Wang, Y. (2019). Improving probabilistic hydroclimatic projections through high-resolution convection-permitting climate modeling and Markov chain Monte Carlo simulations. *Climate Dynamics*, *53*(3–4), 1613–1636. https://doi.org/10.1007/s00382-019-04702-7

Westra, S., Thyer, M., Leonard, M., Kavetski, D., & Lambert, M. (2014). A strategy for diagnosing and interpreting hydrological model nonstationarity. *Water Resources Research*, *50*, 5090–5113. https://doi.org/10.1002/2013WR014719

Winsemius, H. C., Aerts, J. C. J. H., Van Beek, L. P. H., Bierkens, M. F. P., Bouwman, A., Jongman, B., et al. (2016). Global drivers of future river flood risk. *Nature Climate Change*, *6*(4), 381–385. https://doi.org/10.1038/nclimate2893

Yoshikane, T., Kimura, F., Kawase, H., & Nozawa, T. (2012). Verification of the performance of the pseudo-global-warming method for future climate changes during June in East Asia. *Scientific Online Letters on the Atmosphere*, *8*(1), 133–136. https://doi.org/10.2151/sola.2012-033

Yu, K., Zhang, X., Li, P., Li, Z., Qin, Y., & Sun, Q. (2019). Probability prediction of peak break-up water level through vine copulas. *Hydrological Processes*, *33*(6), 962–977. https://doi.org/10.1002/hyp.13377.xia

Zhang, B. (2020). *The hydrological dataset for Guadalupe and Mission river basins over South Texas*. Mendeley Data. http://dx.doi.org/10.17632/csdctns7wj.2

Zhang, B., Wang, S., & Wang, Y. (2019). Copula-based convection-permitting projections of future changes in multivariate drought characteristics. *Journal of Geophysical Research: Atmospheres*, *124*, 7460–7483. https://doi.org/10.1029/2019JD030686

Zhu, J., Wang, S., & Huang, G. (2019). Assessing climate change impacts on human-perceived temperature extremes and underlying uncertainties. *Journal of Geophysical Research: Atmospheres*, *124*, 3800–3821. https://doi.org/10.1029/2018JD029444